China Geology 1 (2021) 77−94

China Geology

Journal homepage: http://chinageology.cgs.cn
https://www.sciencedirect.com/journal/china-geology

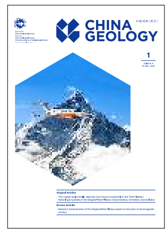

A new understanding of Demala Group complex in Chayu Area, southeastern Qinghai-Tibet Plateau: Evidence from zircon U-Pb and mica $^{40}Ar/^{39}Ar$ dating

Yuan Tang[a, b,*], Yu-ping Liu[b], Peng Wang[b], Wen-qing Tang[b], Ya-dong Qin[b], Xiao-dong Gong[b], Dong-bing Wang[b], Bao-di Wang[b]

[a] *Institute of Geology, Chinese Academy of Geological Sciences, Beijing* 100037, *China*
[b] *Chengdu Center, China Geological Survey, Chengdu* 610081, *China*

A R T I C L E I N F O

Article history:
Received 1 December 2020
Received in revised form 28 February 2021
Accepted 2 March 2021
Available online 8 March 2021

Keywords:
Demala Group complex
Zircon U-Pb dating
$^{40}Ar/^{39}Ar$ dating
Jiali fault zone
Geological survey engineering
Tibet-Qinghai Plateau
China

A B S T R A C T

The Chayu area is located at the southeastern margin of the Qinghai-Tibet Plateau. This region was considered to be in the southeastward extension of the Lhasa Block, bounded by Nujiang suture zone in the north and Yarlung Zangbo suture zone in the south. The Demala Group complex, a set of high-grade metamorphic gneisses widely distributed in the Chayu area, is known as the Precambrian metamorphic basement of the Lhasa Block in the area. According to field-based investigations and microstructure analysis, the Demala Group complex is considered to mainly consist of banded biotite plagiogneisses, biotite quartzofeldspathic gneiss, granitic gneiss, amphibolite, mica schist, and quartz schist, with many leucogranite veins. The zircon U-Pb ages of two granitic gneiss samples are 205 ± 1 Ma and 218 ± 1 Ma, respectively, representing the ages of their protoliths. The zircons from two biotite plagiogneisses samples show core-rim structures. The U-Pb ages of the cores are mainly 644–446 Ma, 1213–865 Ma, and 1780–1400 Ma, reflecting the age characteristics of clastic zircons during sedimentation of the original rocks. The U-Pb ages of the rims are from 203 ± 2 Ma to 190 ± 1 Ma, which represent the age of metamorphism. The zircon U-Pb ages of one sample taken from the leucogranite veins that cut through granitic gneiss foliation range from 24 Ma to 22 Ma, interpreted as the age of the anatexis in the Demala Group complex. Biotite and muscovite separates were selected from the granitic gneiss, banded gneiss, and leucogranite veins for $^{40}Ar/^{39}Ar$ dating. The plateau ages of three muscovite samples are 16.56 ± 0.21 Ma, 16.90 ± 0.21 Ma, and 23.40 ± 0.31 Ma, and the plateau ages of four biotite samples are 16.70 ± 0.24 Ma, 16.14 ± 0.19 Ma, 15.88 ± 0.20 Ma, and 14.39 ± 0.20 Ma. The mica Ar-Ar ages can reveal the exhumation and cooling history of the Demala Group complex. Combined with the previous research results of the Demala Group complex, the authors refer that the Demala Group complex should be a set of metamorphic complex. The complex includes not only Precambrian basement metamorphic rock series, but also Paleozoic sedimentary rock and Mesozoic granitic rock. Based on the deformation characteristics, the authors concluded that two stages of the metamorphism and deformation can be revealed in the Demala Group complex since the Mesozoic, namely Late Triassic-Early Jurassic (203–190 Ma) and Oligocene–Miocene (24–14 Ma). The early stage of metamorphism (ranging from 203–190 Ma) was related to the Late Triassic tectono-magmatism in the area. The anatexis and uplifting-exhumation of the later stage (24–14 Ma) were related to the shearing of the Jiali strike-slip fault zone. The Miocene structures are response to the large-scale southeastward escape of crustal materials and block rotation in Southeast Tibet after India-Eurasia collision.

1. Introduction

Situated between Bangong-Nujiang Suture Zone and Yarlung Zangbo Suture Zone, the Lhasa Block is one of the areas in the Qinghai-Tibet Plateau where the Precambrian rocks are most extensively exposed (BGMRXR, 1993), including the Nyainqentanglha (Li P, 1955; Hu DG et al., 2005; Zhang ZM et al., 2010, 2012a; Zhang XZ et al., 2013), Nyingchi (Yin GH et al., 2006; Dong X et al., 2009; Xu WC et al., 2013; Lin YH et al., 2013), Jiayuqiao (He SP et al.,

* Corresponding author: *E-mail address*: tyvienna@163.com (Yuan Tang).

doi:10.31035/cg2021021

2012) and Demala groups (Peng XJ et al., 1999; Dong YS et al., 2011). The studies on the origin and early tectonic evolution of the Lhasa Block have drawn wide attention in recent years. However, whether or not these groups formed in the Precambrian and their tectonic attributes are still in dispute. For example, the Nyainqentanglha Group distributed in the Nyainqentanglha Mountains and the western part of Namtso area was once considered to be the most ancient metamorphic basement in the Lhasa Block (Li P, 1955; Hu DG et al., 2005; Zhang ZM et al., 2010, 2012a). However, its exact age has not been clearly understood. The zircon U-Pb ages of the orthogneiss in the Nyainqentanglha Group have been reported to be 758−666 Ma (Zhang XZ et al., 2013), 787−748 Ma (Hu DG et al., 2005), 897−886 Ma (Zhang ZM et al., 2012a), and ca. 925Ma (Hu PY et al., 2016). The Cambrian metamorphic rhyolites, ranging from 536 Ma to 492 Ma, were aslo reported in Yongzhu and Nima areas (Hu PY et al., 2013; Zhu DC et al., 2012; Pan XP et al., 2012; Ding HX et al., 2015). These ages indicated that the Nyainqentanglha Group can be a set of Precambrian rocks. However, the composition of the Nyainqentanglha Group is complicated, including oceanic crust or island arc origin orthogneiss and volcanic rocks, and continental origin paragneiss, quartzite and slate (Hu DG et al., 2003; Zhang XZ et al., 2013; Hu PY et al., 2013; Zhu DC et al., 2012; Pan XP et al., 2012). Therefore, the Precambrian tectonic evolution of Lhasa block is very confused and needs to be studied more deeply and systematically.

The Chayu area, located in the eastern part of the great turn of Yarlung Zangbo River, is considered to be in the southeastward extension of the Lhasa Block (Li YC et al., 2018; Fig. 1a). In this area, the widely distributed high grade metamorphic gneiss series of the Demala Group complex were inferred as Precambrian metamorphic basement of the Lhasa Block (Peng XJ et al., 1999; Dong YS et al., 2011). The Demala Group complex was formerly known as Precambrian Bomi gneiss (Li P, 1955), Bomi-Chayu complex (BGMRXR, 1993), and Chayu Group (Luo JN, 1992). In the 1∶200000 regional geological survey of Songleng and Zhuwagen map sheets in 1995, the Sm-Nd ages of 2145.96−2264.06 Ma and 1524.46−1598.01 Ma and the Sm-Nd isochron age of 2138 Ma were obtained. Accordingly, the Paleo−Mesoproterozoic Mosetong Formation and Sheduo Formation were newly established and combined into Demala Group complex. In the subsequent 1∶250000 regional survey (GSITAR, 2007[①]), it was suggested that the Demala Group complex is a set of medium-high grade metamorphic rock series and composed of schist, leptynite, gneiss, amphibolite and marble. The protoliths of the Demala Group complex are a set of thick marine sedimentary rocks, including aluminum rich clay rock, silicon rich argillaceous clastic rock and carbonate rock. Dong YS et al. (2011) conducted zircon U-Pb dating and biotite $^{40}Ar/^{39}Ar$ dating of schists in the Demala Group complex, indicating that the Demala Group complex contains Paleozoic sedimentary rocks intruded by Mesozoic magma. They were modified by metamorphism and magmatism in the Cenozoic (Dong YS et al., 2011).

In this paper, the rock composition and structural characteristics of the Demala Group complex were investigated based on field structural and microstructural analysis. LA-ICP-MS zircon U-Pb dating was used to the gneisses of the Demala Group complex. Biotite and muscovite were selected from deformed gneiss for $^{40}Ar/^{39}Ar$ dating.

2. Geological setting

2.1. Regional tectonic framework

The geological frame of the Chayu area is shown in Fig.1b and Fig.1c. As the key research object of this paper, the Demala Group complex is distributed in a banded form in NNW or nearly SN trending. It is comparative to the Nyingchi Group to the west of the eastern Namche Barwa Syntaxis towards the northwest (Dong X et al., 2009) and comparative to Gaoligong Group in west Yunnan and the Mogok gneiss in Burma towards the south (Tang Y et al., 2020). The Neoproterozoic-Cambrian Bomi Group distributed along Ranwu-Chayu area is a set of clastic rocks interbedded with volcanic rocks, which underwent greenschist facies metamorphism and fold deformation (Xie YW et al., 2007). The sporadic Ordovician strata and banded Devonian strata are a set of sedimentary caprocks dominated by limestone. The Carboniferous-Permian gravel-sand-bearing slates interbedded with a few volcanics are widely distributed in the central part of the area. The Mesozoic-Early Tertiary strata are mainly distributed along Nujiang River in the north or are deposited along intermountain basins. Granite is widely distributed in this area. All Early Mesozoic or Pre-Mesozoic cap rocks and metamorphic rock series were intruded and modified by these granitic rocks, which were the Meso-Cenozoic intrusion (Chiu HY et al., 2009; Zhu DC et al, 2009; Pan FB et al., 2012; Li HQ et al., 2012). In this region, it is characterized by extensive strike-slip shear zones or faults, such as the Parlung and Puqu strike-slip faults considered to be branches of the Jiali fault (Fig. 1c; Lee HY et al., 2003; Lin TH et al., 2009; Zhang B et al., 2020).

2.2. Characteristics of rock association in Demala Group complex

Based on field-based investigations and microstructural analysis, it can be concluded that the Demala Group complex is mainly consisted of medium-high grade metamorphic rock series, including gneiss, schist, amphibolite, leptynite and marble.

The gneiss is featured by banded gneiss and biotite

[①] *GSITAR(Geological Survey Institute of Tibet Autonomous Region). 2007. 1∶250000 regional geological survey report of Chayu (Non public publications).*

monzogneiss, biotite plagiogneisses, biotite quartzofeldspathic gneiss (Figs. 2a, c−h), as well as augen-like or gneissic granitic gneiss (Figs. 2b, i, j) in the Demala Group complex. Its mineral constituents include plagioclase (28%−50%), potash feldspar (0−50%), biotite (10%−30%), and quartz (16%−25%). With strong migmatization, many leucogranite veins have developed along or cutting through foliation (Figs. 2e−h). Gneissic foliation is generally in NNW strike, with a high dip angle (about 40°−60°; Figs. 2a, c, d). Meanwhile, mineral lineation is formed by arranged minerals, including mica, feldspar and quartz. The lineation is a dip direction of 130°−160° and a dip angle of 15°−30° (Fig. 1d). According to the microscopic observation of the gneiss, the quartz and its aggregates show polycrystalline ribbons or/and rectangular monocrystal grains (Figs. 3a−f). Feldspar porphyroclasts show bulging recrystallization on the rim (Figs. 3b, c, f), or mosaic new grain aggregates (Figs. 3d, e). The micas develop around feldspar porphyroclast (Figs. 3b, c, f) or are

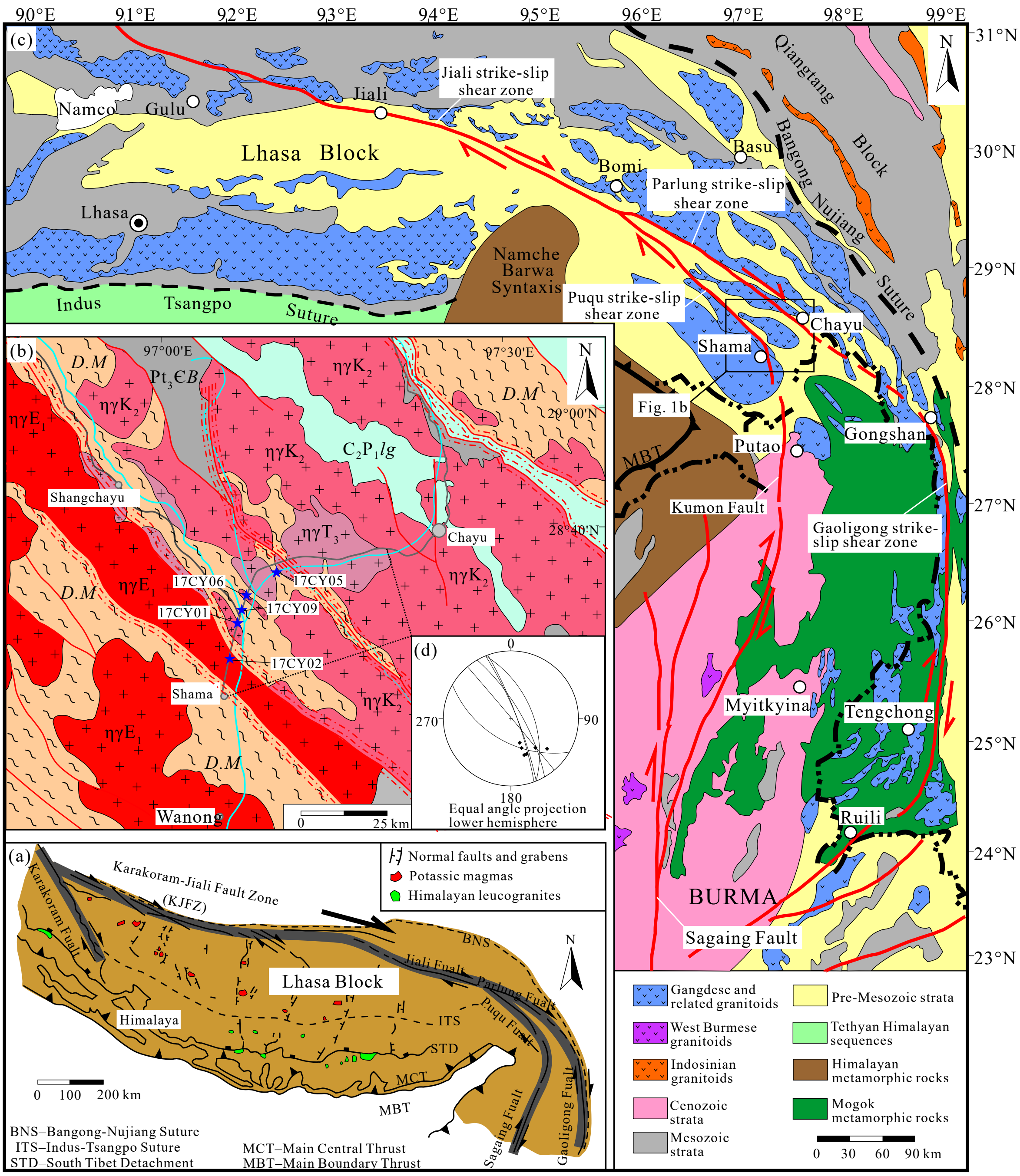

Fig. 1. a−Schematic tectonic map of the Himalayas and southern Tibet (modified from Lee HY et al., 2003). b−Generalized geological map of Chayu area. *D.M*−Demala metamorphic complex: Gneiss, schist; $Pt_3\epsilon B$−Neoproterozoic-Cambrian Bomi group: Schist, meta sandstone, slate, phyllite; C_2P_1lg−Upper Carboniferous−Permian Laigu group: Slate, sandstone, limestone; $\eta\gamma T_3$−Late Triassic monzogranite; $\eta\gamma K_2$−Late Cretaceous monzogranite; $\eta\gamma E_1$−Paleogene monzogranite; blue star, indicating sampling location. c−Simplified geological map of the Jiali fault zone, Eastern Tibet (modified from Lee HY et al., 2003). d−Stereogram of the foliation (large circular arc) and mineral stretching lineation (black dot) for observing sites along the cross-section Chayu-Shama.

discontinuously arranged parallel to quartz ribbons (Figs. 3d, e). S-C fabric and mica fish are well developed in the gneiss (Fig. 3b), indicating that the rock experienced dextral shear.

The schist in the Demala Group complex mainly includes two-mica schist, two-mica quartz schist, feldspar-biotite schist, and hornblende-biotite schist, with granular lepidoblastic texture and flaky structure (Figs. 4a, b). Quartz, mica and feldspar are the main minerals of the schists. The amphibolite in the Demala Group complex exhibits medium-fine columnar-granular crystalloblastic texture and of blocky or flaky structures (Fig. 4c). Its mineral assemblage consists of hornblende (30%−40%), plagioclase (35%−50%), biotite (2%−16%), quartz (0−3%), and potash feldspar (0−5%), with diopside (0−12%) visible locally. The leptynite in the Demala Group complex mainly includes biotite-monzonite leptynite and biotite-plagioclase leptynite, with granular lepidoblastic texture and blocky or weakly directional structures (Fig. 4d). Its mineral assemblage consists of plagioclase (15%−75%), potash feldspar (0−50%), quartz (10%−30%), and biotite (5%−15%). The marble of the Demala Group complex is of

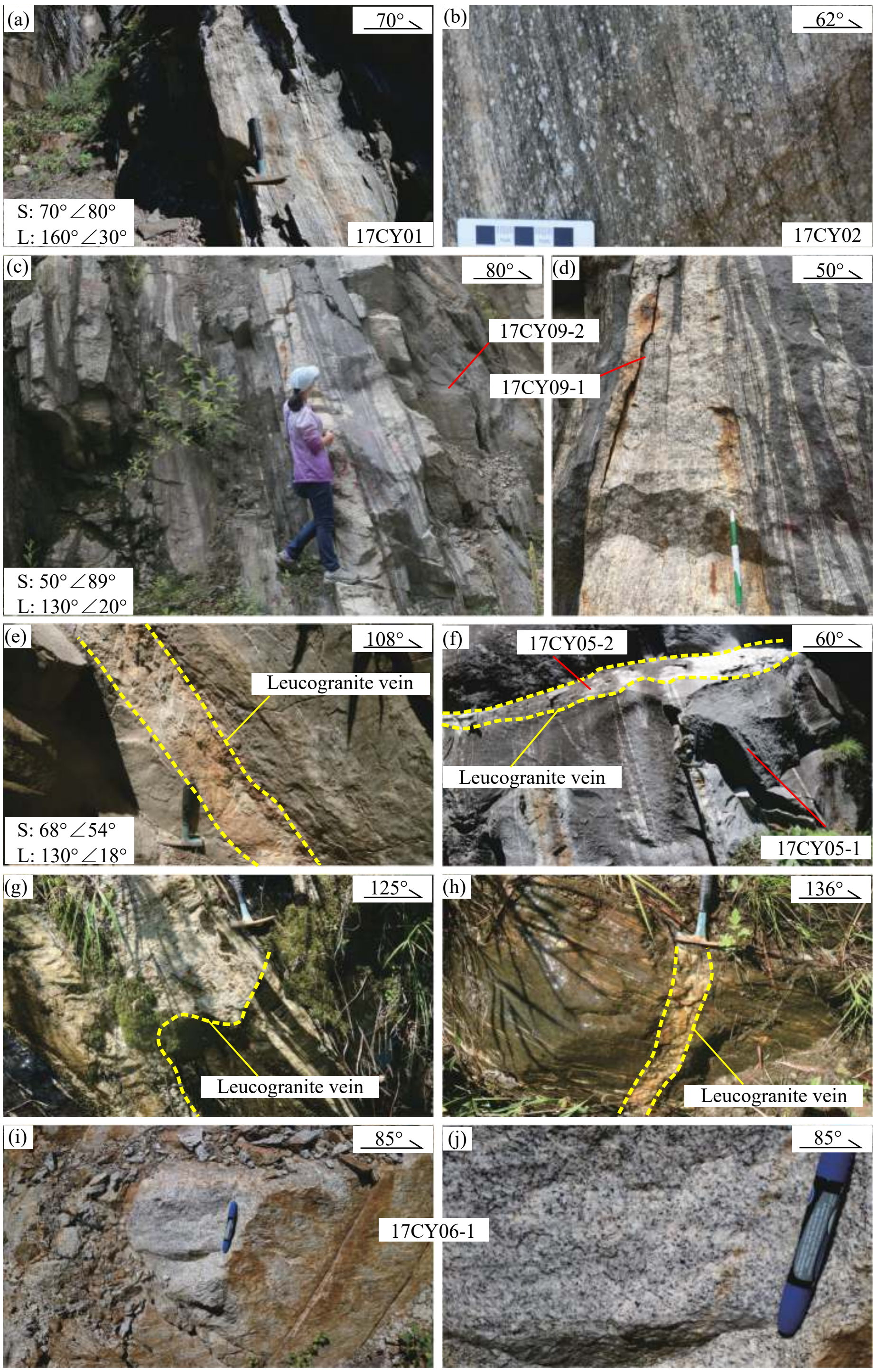

Fig. 2. Outcrop structural characteristics of the Demala Group complex.

fine-grained granular crystalloblastic texture and blocky or striped structures. Its mineral constituents include calcite (50%−80%) and quartz (10%−30%). Following a microscopic observation, the mica minerals in two-mica schist are directionally arranged, and the mica fish formed from muscovite indicate dextral shear (Fig. 4a); S-C fabric develops in the amphibolite (Fig. 4c), of which the foliation S is formed from the directional arrangement of lenticular hornblende porphyroclast, and the shears C are formed from the directional arrangement of aggregates consisting of acicular hornblende, flaky biotite, and granular plagioclase that are newly generated owing to dynamic recrystallization. The S-C fabric also indicates dextral shear.

3. Analytical methods

3.1. Zircon U-Pb dating

In this paper, five gneiss samples (17CY01, 17CY09-1, 17CY09-2, 17CY05-1, 17CY05-2; relative sampling locations shown in Fig. 1b) were selected from Chayu-Shama section for LA-ICP-MS zircon U-Pb dating. Zircons were separated at the laboratory of the Hebei Institute of Regional Geological and Mineral Resource Survey, The CL images of zircons were taken in the Wuhan Sample Solution Analytical Technology Co., Ltd. using the high-vacuum scanning electron microscope (JSM-IT100) equipped with GATAN MINICL system. The operating voltage was 10.0−13.0 kV and the

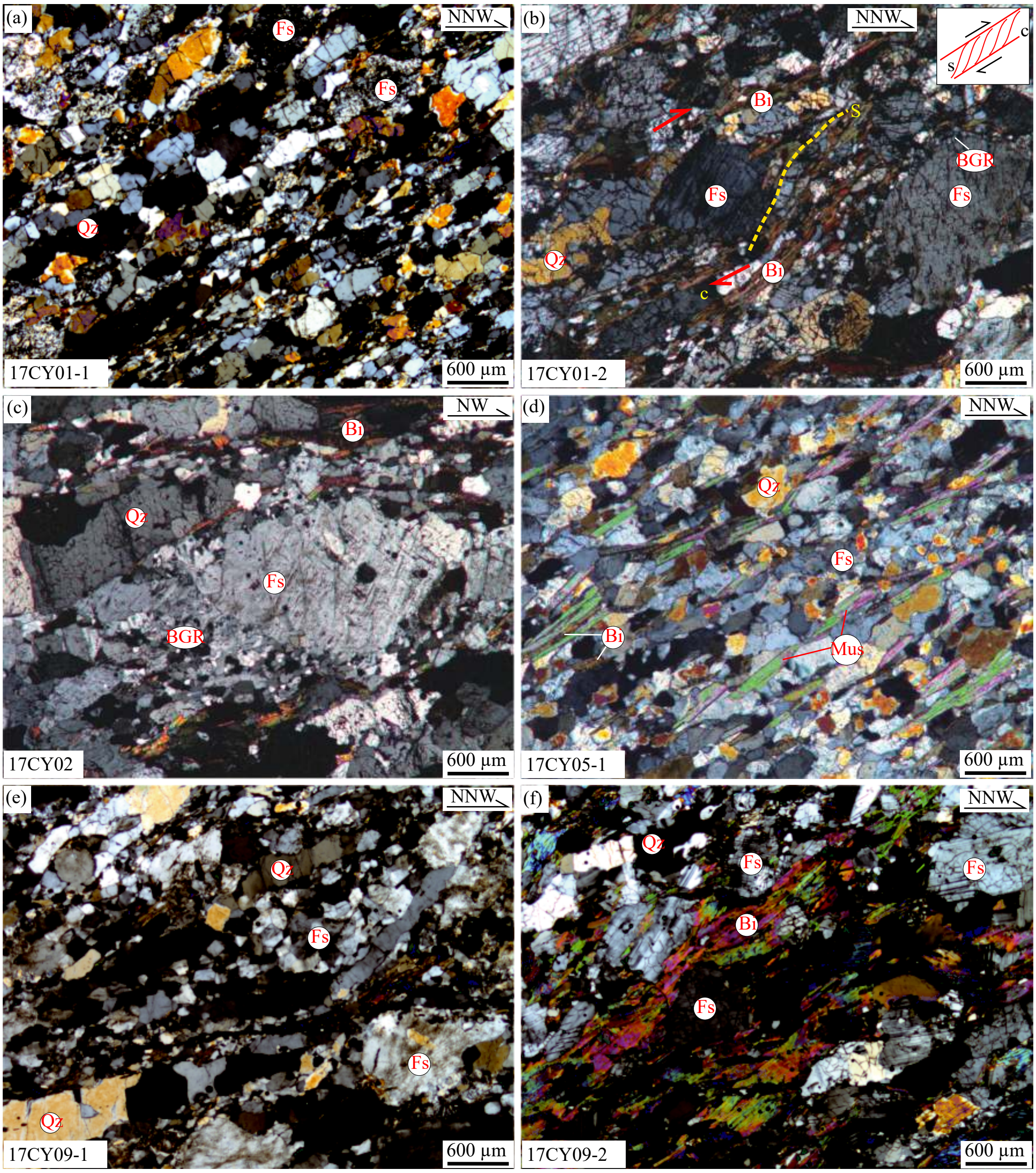

Fig. 3. Microstructural characteristics of gneiss in the Demala Group complex; Fs−feldspar, Qz−quartz, Mus−muscovite, Bi−biotite, BGR−bulging recrystallized feldspar.

current of the tungsten filament was 80−85 μA.

Zircon U-Pb isotope dating and trace-element content analysis were conducted by LA-ICP-MS in the Wuhan Sample Solution Analytical Technology Co., Ltd at the same time (see Zong KQ et al., 2017 for detailed instrument parameters and analysis process). The GeolasPro laser ablation system consisting of an excimer laser at 193 nm wavelength (COMPexPro 102 ArF) and a MicroLas optical system was used as the LA-ICP-MS laser ablation system. Meanwhile, the Agilent 7700e ICP-MS was adopted for ICP-MS. During laser ablation, helium was used as carrier and argon as complemental air to regulate the sensitivity. They were mixed via a T-shaped joint before entering ICP. The laser ablation system was equipped with a signal smoothing device (Hu ZC et al., 2015). The beam spot diameter and frequency were 32 μm and 5 Hz, respectively. Zircon reference material 91500 and glass reference material NIST610 were taken as external reference materials for fractionation correction of isotopes and trace elements, respectively. Each time, the resolution-based analytical data includes a blank signal of about 20–30 s and a sample signal of 50 s. The analytical data processing (including selection of sample signals and blank signals, correction of sensitivity drift of instruments, calculation of element content, and the calculation of U-Pb isotope ratio and ages) was carried out off-line by ICPMSDataCal program (Liu YS et al., 2008, 2010). Isoplot/Ex_ver3 (Ludwig KR, 2003) was used to plot the concordance line of U-Pb ages of the zircon samples and to calculate the weighted average age.

3.2. Mica Ar-Ar dating

Biotite and muscovite were separated from metamorphic rocks of the Demala Group complex for $^{40}Ar/^{39}Ar$ dating. The mineral separates were selected at the lab of Hebei Institute of Regional Geological and Mineral Resource Survey and the $^{40}Ar/^{39}Ar$ dating was carried out at the isotope thermochronological lab of the Institute of Geology, Chinese Academy of Geological Sciences. After ultrasonic cleaning, the cleaned pure mineral samples (purity > 99%) were encapsulated in quartz vials. This package was then placed into a nuclear reactor and irradiated with neutrons. The samples were irradiated in the Swimming Pool Reactor at the Institute of Atomic Energy, Chinese Academy of Sciences. Using channel B4, the reactor delivered a neutron flux of about 26.5×10^{12} n/cm^{2}S. The total irradiation time was 1440 min and integral neutron flux was 2.29×1018 n /cm^2. Meanwhile, a biotite reference sample ZBH-25 (132.7 ± 1.2 Ma, and 7.6% K) was irradiated with neutrons together as acontrol sample.

A graphite furnace was used for step-heating of the samples, during which the samples were heated for 10 min and purified for 20 min for each temperature increment. Mass spectrometry was carried out using a multicollector noble gas mass spectrometer Helix MC, with 20 sets of data collected

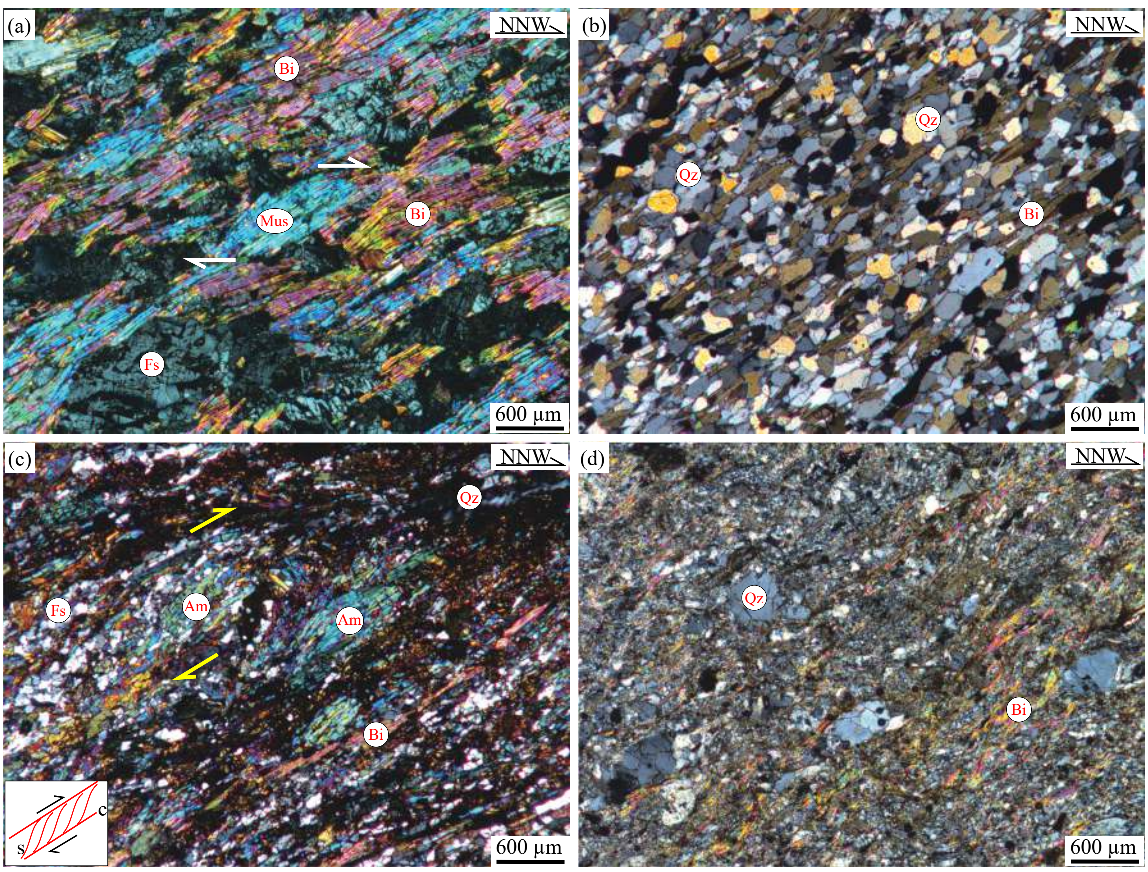

Fig. 4. Microstructural characteristics of the Demala Group complex; a−mica schist, b−quartz schist, c−amphibolite, d−biotiteleptynite; Fs−feldspar, Qz−quartz, Mus−muscovite, Bi−biotite, Am-amphibole.

for each peak value. Mass discrimination correction, atmospheric argon correction, blank correction, and interfering isotope correction were conducted for all data after they were regressed to the time zero values. The interfering isotope correction factors produced in the process of neutron irradiation were obtained by analyzing the irradiated K_2SO_4 and CaF_2 and they are $(^{36}Ar/^{37}Ar_o)_{Ca}$=0.0002398, $(^{40}Ar/^{39}Ar)_K$= 0.004782, and $(^{39}Ar/^{37}Ar_o)_{Ca}$ =0.000806. Radioactive decay correction was carried out for ^{37}Ar and the ^{40}K decay constant λ is 5.543×10^{-10} /a (Steiger RH et al., 1977). The plateau ages, isochrone ages, and inverse isochrone ages were calculated with the program Ar-Ar CALC (Anthony Koppers, v2.5.2, 2012), with errors within 2σ. Detailed experimental processes are stated in relevant articles (Chen W et al., 2006; Zhang Y et al., 2006).

4. Samples and results

4.1. Zircon U-Pb dating

The sample 17CY01 was taken from banded biotite quartzofeldspathic gneiss (Fig. 2a). According to the microscopic observation of the sample, the quartz mainly appears as rectangular polycrystalline ribbons (Figs. 3a, b), the feldspar is mainly xenomorphic granular in shape (Figs. 3a, b), and the biotite is flaky in shape and directionally arranged (Fig. 3b). All these indicate that this set of rocks are paragneiss and their protoliths may be a set of sedimentary clastic rocks. The zircons from sample 17CY01 show an ordinary automorphic degree and are long or short columnar in shape. The CL images of the zircons indicate that all the zircons have core-rim structure (Fig. 5a). The cores are relatively wider, more than 60 μm generally. Some rims are wide, about 30−40 μm (Fig. 5a), and others are narrow (Fig. 5b), less than 10 μm in general. The cores are highly luminous. Some of them have no obvious texture, while others have residual irregular oscillatory zoning. The rims are weakly luminous, and most of them show regular oscillatory zoning. The contact parts between the rims and the cores are in the shapes of scraggly bays and saw-teeth. These structures of the zircons indicate that the cores are the residual zircons in the protolith unaffected by metamorphism, while the rims were formed owing to later metamorphism. In this study, 20 zircon grains with wide rims were selected for dating (Fig. 5a), and 18 effective analysis points were obtained. The content of Th and U is 24.4×10^{-6}−194.4×10^{-6} and 1409×

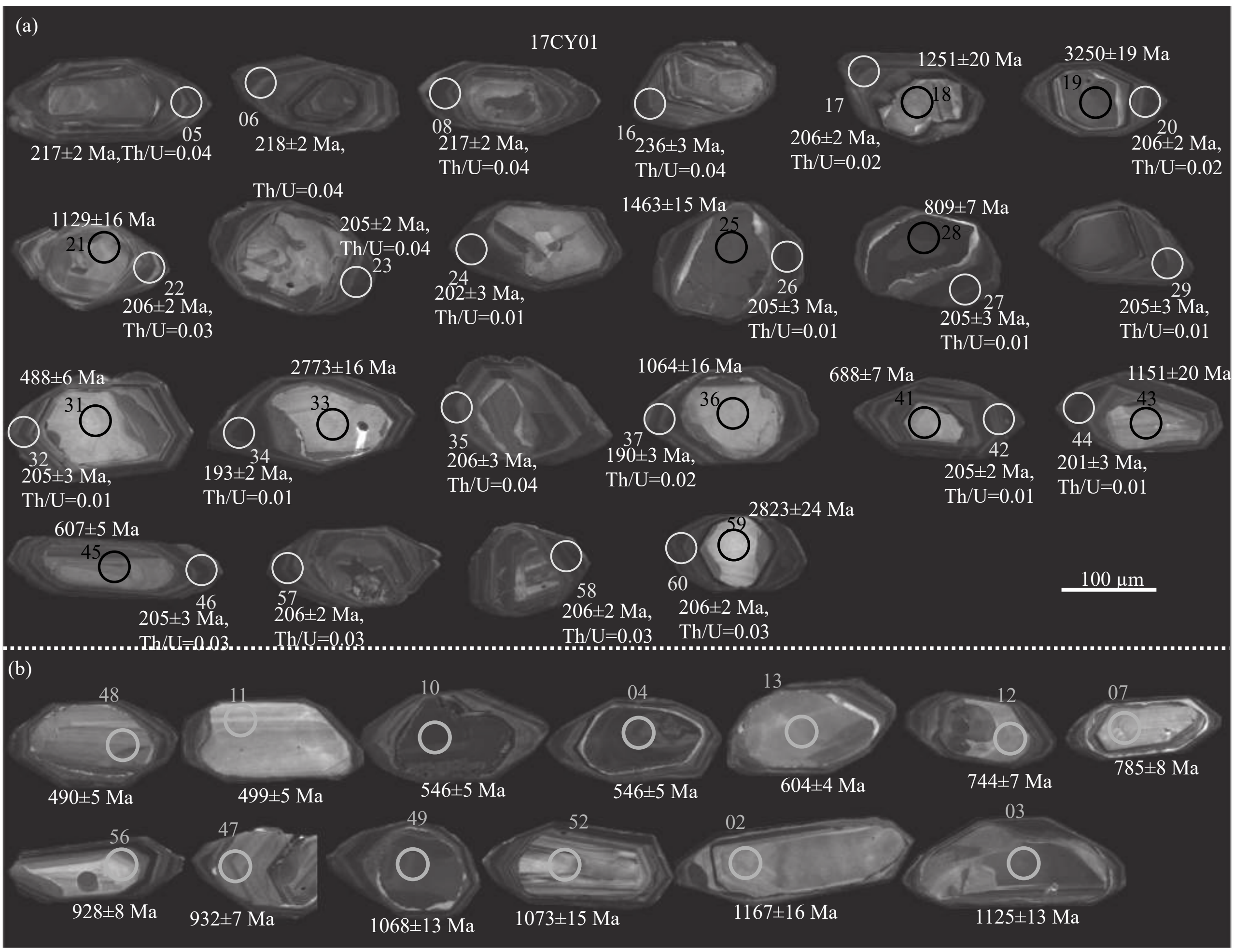

Fig. 5. Cathodoluminescence (CL) images of representative zircons from the Sample 17CY01. a−zircons with wide rim dated $^{206}Pb/^{238}U$ age around 203 Ma; b−zircons with narrow rim. Circles with data indicate spots and ages of LA-ICP-MS dating. The diameters of the circles are 32μm.

10^{-6}–3914×10^{-6}, respectively, indicating low Th content and high U content. Meanwhile, the mean Th/U ratio is 0.02 (detailed data in supplementary Table S1; Fig. 6b), indicating the characteristics of metamorphic zircons (Wu YB and Zheng YF, 2004). The 18 analytical points of the sample mostly fall on or near the U-Pb concordia curve (Fig. 6a). Furthermore, the $^{206}Pb/^{238}U$ weighted mean age is 203 ± 2 Ma (MSWD=3.6, n=18, Fig. 6a), representing the age of

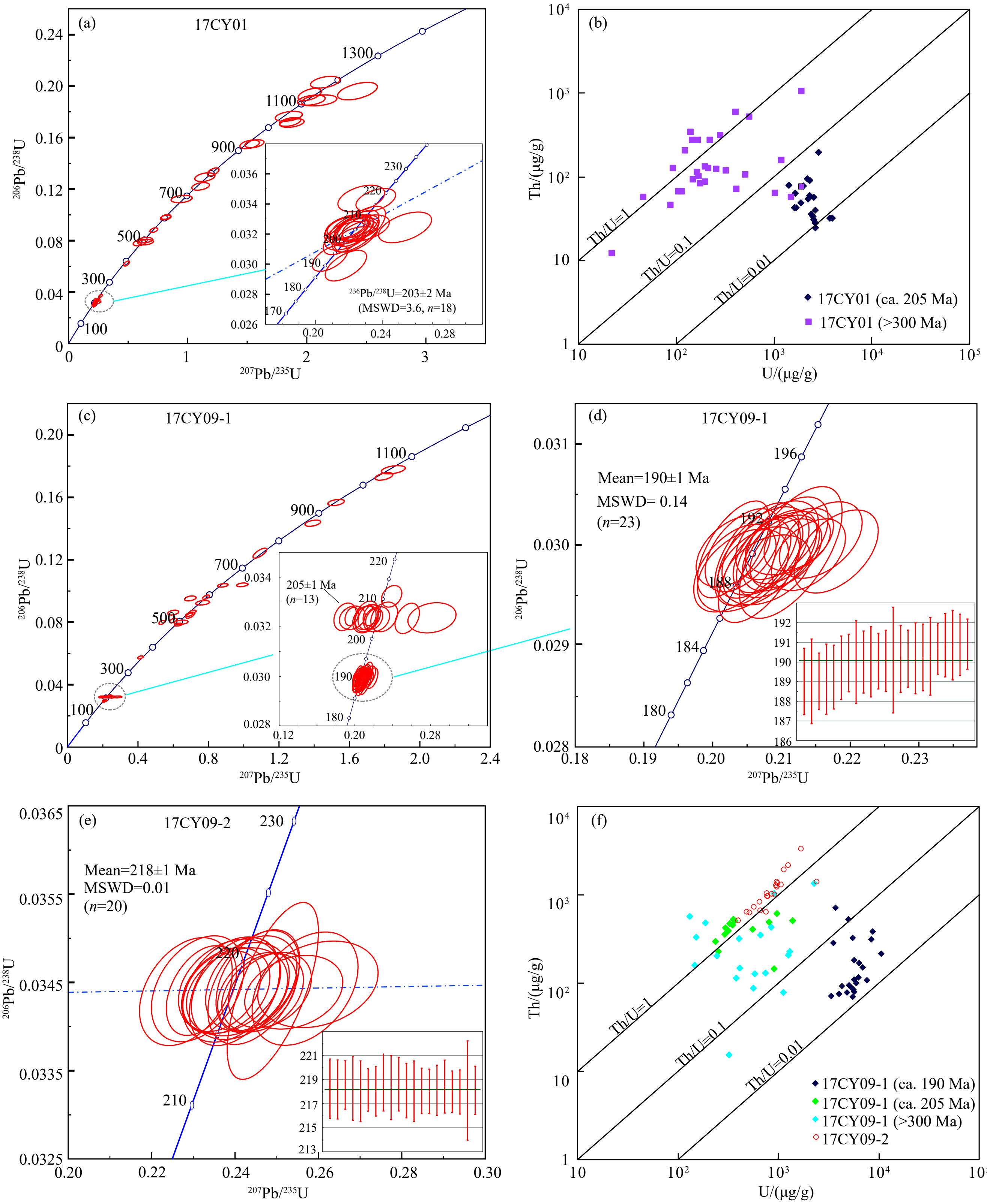

Fig. 6. a–Zircon U-Pb concordia diagrams of Sample 17CY01; b–content of Th and U and Th/U ratios of zircons from Sample 17CY01; c–e–zircon U-Pb concordia diagrams of samples17CY09-1 and 17CY09-2; f–content of Th and U and Th/U ratios of zircons from samples 17CY09-1 and 17CY09-2.

metamorphism of quartzofeldspathic gneiss. In addition, 40 zircon cores without fissures and obvious inclusions were selected for dating, obtaining 30 effective analytical points, and the isotope ratios and age results are shown in supplementary Table S1 and Fig. 6a. Most of the analysis points have high age concordance. The Th/U ratios are greater than 0.1 (Fig. 6b), which shows the characteristics of magmatic zircon. The ages determined fall within a wide range of 2800−480 Ma and are mainly distributed in two ranges, namely 850−480 Ma and 1300−1100 Ma. The ages, beyond 1300 Ma, are distributed in a scattered manner, representing the age characteristics of clastic zircons during sedimentation of the protoliths.

The samples 17CY09-1 and 17CY09-2 were taken from one outcrop with the lithology of banded gneiss. The dark bands of the outcrop mainly consist of biotite granitic gneiss, while the light ones mainly include quartzofeldspathic gneiss. Furthermore, the quartzofeldspathic bands show flowage folds or rootless hook folds locally, whose axial-plane is parallel to the foliation of gneiss (Figs. 2c, d). In this study, samples were taken from both the light and dark bands. Among them, the sample 17CY09-1 was taken from the light bands. It mainly contains quartzofeldspathic rocks according to microscopic observation. The quartz in the sample appears as monocrystalline ribbons or rectangular megacrystalline ribbons, and the feldspar in the sample appears as porphyroclasts or recrystallized new grains, with static triplets visible. These indicate that the rocks in the sample experienced static restoration and recrystallization at a high temperature (Fig. 3e). The zircons of the sample have a high degree of automorphism. Most of them are long columnar and a few are short columnar. As shown in the CL images (Fig. 7), most of the zircons have core-rim structure, with all rims being weakly luminous. According to the characteristics of cores and rims, the zircons of this sample can be classified into two types: (1) The zircons composed of relict cores with

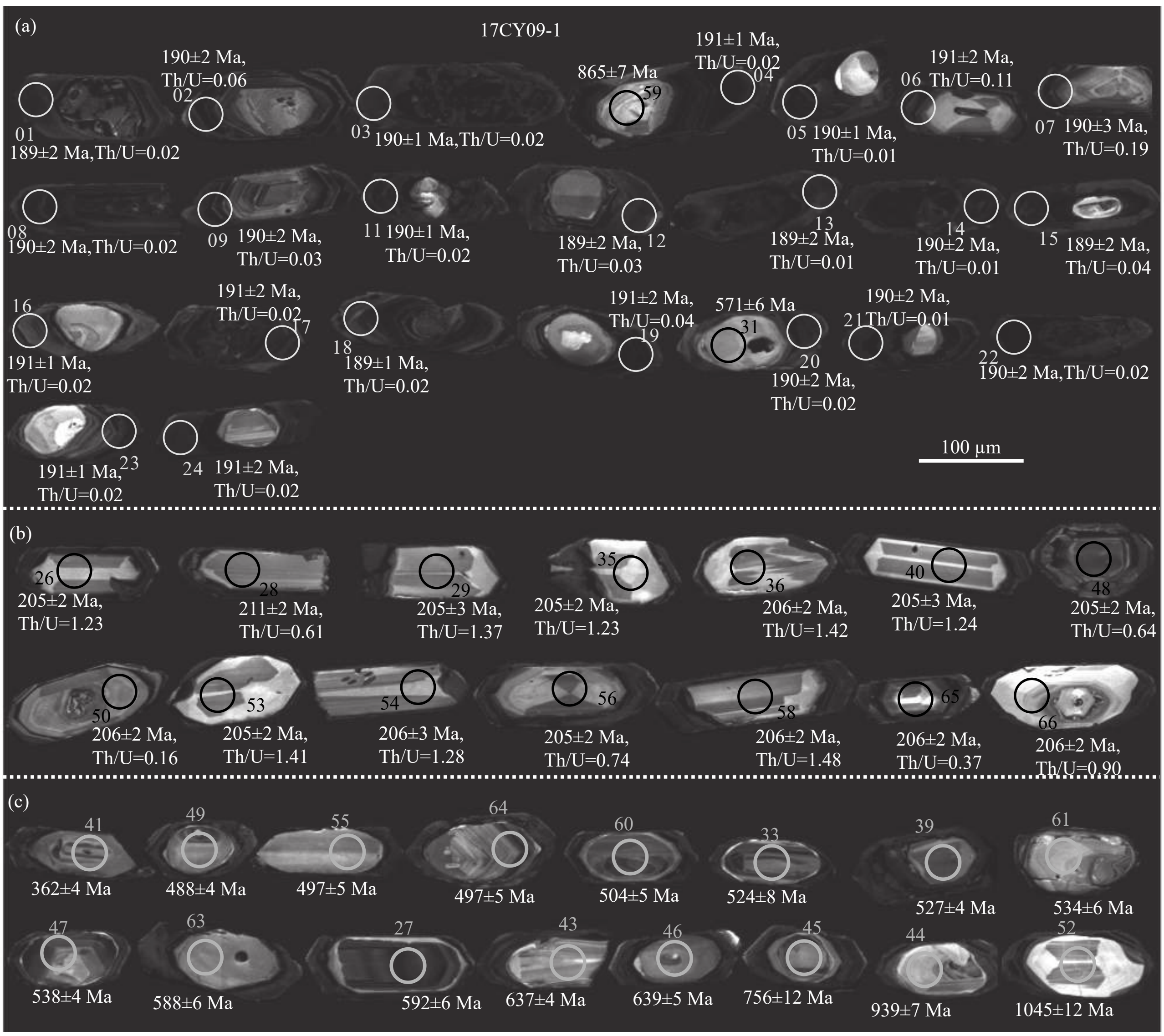

Fig. 7. Cathodoluminescence (CL) images of representative zircons from the Sample 17CY09-1. a−zircons dated $^{206}Pb/^{238}U$ age around 190 Ma; b−zircons dated $^{206}Pb/^{238}U$ age around 205 Ma; c−zircons dated $^{206}Pb/^{238}U$ age older than 300 Ma. Circles with data indicate spots and ages of LA-ICP-MS dating. The diameters of the circles are 32μm.

strong luminescence and metamorphic overgrowth rims (e.g. the zircons at points Nos. 4, 5, 15, 16, 19, 20 and 23 in Fig. 7a); (2) the zircons with transformed original part serving as the rims and untransformed original part as the cores (e.g. zircons at points Nos. 1, 2, and 9 in Fig. 7a and zircons in Fig. 7b). Compared to the zircons of the first type, the zircons of the second type are less luminous and show planar or fan-shaped zoning or no zoning. They were formed possibly owing to metamorphic recrystallization (Wu YB and Zheng YF, 2004). In this paper, 24 zircons with wide rims were selected for dating (Fig. 7a), obtaining 23 effective analytical points. The content of Th and U is 70.1×10^{-6}−708.1×10^{-6} and 3336×10^{-6}−10652×10^{-6}, respectively, indicating low Th content and high U content. Meanwhile, the mean Th/U ratio is 0.04 (supplementary Table S1; Fig. 6f), indicating the characteristics of metamorphic zircons (Wu YB and Zheng YF, 2004). The 23 effective analytical points on zircon rims of the sample 17CY09-1 mostly fall on or near the U-Pb concordia curve (Fig. 6c). The $^{206}Pb/^{238}U$ weighted mean age is 190 ± 1 Ma (MSWD=0.14, n=23; Fig. 6d), representing the metamorphism age of the quartzofeldspathic gneiss. In addition, some cores of zircon grains were selected for U-Pb dating. A total of 48 effective analytical points were obtained and most of them fall on or near the U-Pb concordia curve (Fig. 6c). Among them, 13 dating points are mainly around 205 Ma (Figs. 6c, 7b). The contents of Th and U in these 13 zircons are 147×10^{-6}−619×10^{-6} and 235×10^{-6}−1387×10^{-6} respectively (supplementary Table S1). The average Th/U ratio is 1.04 (Fig. 6f), which indicates that these 13 zircons have the characteristics of magmatic zircons (Wu YB and Zheng YF, 2004). Meanwhile, their zircon $^{206}Pb/^{238}U$ weighted mean age is 205 ± 1 Ma (MSWD=0.03, n=13; the right bottom corner of Fig. 6c). The zircon U-Pb ages of the remaining analytical points scatter in a wide range of 473−2696 Ma (Figs. 6c, 7c; supplementary Table S1).

The sample 17CY09-2 was taken from the dark bands of the banded gneiss. According to microscopic observation, it mainly consists of minerals such as biotite, feldspar, and quartz. The feldspar in the sample is porphyroclastic in shape and the quartz appears as ribbons. Therefore, the protolith of the sample should be a set of granite (Fig. 3f). The zircons of the sample show an ordinary automorphic degree, generally in the form of long columns with a long axis diameter of 120 μm. As shown in the CL images (Fig. 8a), the zircons have no core-rim structure and generally show planar zoning or no zoning. Meanwhile, most of the zircons show narrow highly bright bay-like corroded rims, indicating that they experienced hydrothermal reaction (Wu YB and Zheng YF, 2004). For the 20 zircon checked points of the sample 17CY09-2, the contents of Th and U are 513×10^{-6}−3345×10^{-6} and 401×10^{-6}−2411×10^{-6} respectively, and the mean Th/U ratio is 1.28 (Fig. 6f; supplementary Table S2), indicating the characteristics of magmatic zircons (Wu YB and Zheng YF, 2004). The 21 analytical points of the sample mostly fall on or nearby the U-Pb concordia curve (Fig. 6e). The $^{206}Pb/^{238}U$ weighted mean age is 218 ± 1 Ma (MSWD=0.01, n=20), which was interpreted as the crystallization age of the protoliths of granitic gneiss in the complex.

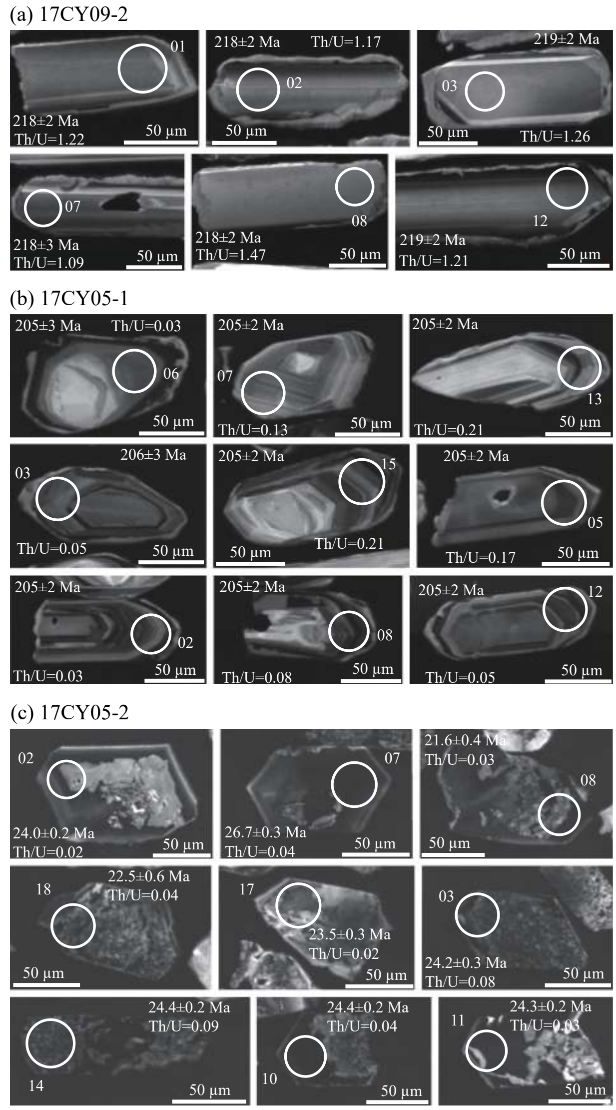

Fig. 8. Cathodoluminescence (CL) images of representative zircons from the samples 17CY09-2, 17CY05-1 and 17CY05-2. Circles with data indicate spots and ages of LA-ICP-MS dating. The diameters of the circles are 32 μm.

The samples 17CY05-1 and 17CY05-2 were taken from one outcrop (Fig. 2f). The lithology of the sample 17CY05-1 is characterized by grayish black granitic gneiss, with foliation developing. According to microscopic observation, the rocks of the sample 17CY05-1 show banded structure in general, the quartz is mainly rectangular megacrystalline ribbons, and the feldspar mainly appear as recrystallized neograins with visible static triplet. All these indicate that the sample experienced static recrystallization at a high temperature (Fig. 3d). The zircon grains of the sample 17CY05-1 are mainly dark-yellow or colorless, with grease-glass luster and good transparency. Most of them are subhedral-euhedral, with a long-axis diameter of 80−120 μm. As indicated by the CL image (Fig. 8b), the zircons show the core-rim structure composed of highly luminescent inherited core and magmatic oscillatory zoning. These characteristics indicate that zircons are not affected by the later deformation metamorphism. The zones in the magmatic oscillatory zoning without fissures and distinct inclusions were selected to obtain analytical points (Fig. 8b). For the 14 zircon analytical points of the sample 17CY05-1, the contents of Th and U are 88.5×10^{-6}–864.5×10^{-6} and 614×10^{-6}–4131×10^{-6}, respectively, and the mean Th/U ratio is 0.18 (supplementary Table S2), indicating the characteristics of magmatic zircon (Wu YB and Zheng YF, 2004). All of the 14 checked points fall on or near by the U-Pb concordia curve (Fig. 9a), and the $^{206}Pb/^{238}U$ weighted mean age is 205 ± 1 Ma (MSWD=0.01, *n*=14; Fig. 9a), which can represent the age of the protoliths of granitic gneiss.

The sample 17CY05-2 was taken from a leucogranite vein that cuts through the foliation of the granitic gneiss. Most zircons of the sample show a high euhedral degree and are in the shape of long columns. As shown in the CL image (Fig. 8c), the crystals in the sample are weakly luminous in general; most of them show fog-like or spongy characteristics inside, with the oscillatory zoning still visible on zircon rims. The zones of zircon rims without fissures and obvious inclusions were selected to obtain analytical points. For the 16 analytical points of the sample, the contents of Th and U are 92×10^{-6}–5086×10^{-6} and 4286×10^{-6}–56692×10^{-6}, respectively, and the Th/U ratios are all less than 0.1 and mostly 0.02−0.04 (supplementary Table S2). Most of the 16 analytical points fall on or nearby the U-Pb concordia curve (Fig. 9b) and the $^{206}Pb/^{238}U$ ages of the sample are 20.6–26.7 Ma. Since the $^{206}Pb/^{238}U$ ages range widely, their weighted mean age has little scientific significance. However, the age distribution histogram (Fig. 9b) is mainly 24−22 Ma. These zircon characteristics are generally consistent with those of the leucogranite veins in high-grade metamorphic rock areas and migmatization areas formed owing to anatexis (Wu YB and Zheng YF, 2004; Dong HW et al., 2014; Tang Y et al., 2016). Therefore, the zircon U-Pb ages of 22−24 Ma represent the anatexis age of the sample17CY05-2.

4.2. Mica Ar-Ar dating

The detailed Ar-Ar dating results of micas through step-heating experiments are shown in supplementary Table S3.

As for the sample 17CY01, biotite separates were selected for $^{40}Ar/^{39}Ar$ dating. The total gas age is 16.63 Ma, and eight steps from 760°C to 1180°C comprise a well-defined age plateau (Fig. 10a). The plateau age is 16.70 ± 0.24 Ma, corresponding to 92.3% of ^{39}Ar release. The $^{36}Ar/^{40}Ar$-$^{39}Ar/^{40}Ar$ isochrone age is 16.68 ± 0.38 Ma (Fig. 10b). The initial $^{40}Ar/^{36}Ar$ is 396.9 ± 18.6 (MSWD=2.9), higher than Nier value, indicating the presence of excess argon. According to microscopic observation, the biotites in the sample are oriented parallel to the gneissic foliation and the stretching lineation of other minerals such as feldspar (Fig. 3b). This indicates that the biotites were formed as a result of deformation and metamorphism at temperature about 550−650°C. As the closure temperatures for biotite Ar-Ar isotopic systems is 320±40°C (Harrison TM et al., 1985), below the deformation temperature, the Ar-Ar age of biotites record the exhumation and/or cooling event that the sample 17CY01 experienced. Biotites separated from the sample 17CY02 were chosen for $^{40}Ar/^{39}Ar$ dating. The total gas age is 16.12 Ma, and 10 steps from 720°C to 1150°C comprise a well-defined age plateau (Fig. 10c). The plateau age is 16.14 ± 0.19 Ma, corresponding to 99.3% of ^{39}Ar release. The $^{36}Ar/^{40}Ar$-$^{39}Ar/^{40}Ar$ isochrone age is 16.22 ± 0.23 Ma (Fig. 10d). The initial $^{40}Ar/^{36}Ar$ is 286.4 ± 15.9 (MSWD=1.1), comparable to Nier value, indicating that there is no excess argon. The sample consists of granitic gneiss. As indicated by hand specimen, the feldspar appears as augen porphyroclasts and is discontinuously arranged to form gneissic foliation, and the biotite aggregates are arranged parallel to the foliation (Fig. 2b). This suggests that the biotite was formed in the process of deformation at about 550°C. Because the closure temperature of biotite is lower than the deformation temperature, the Ar-Ar age results can reflect the exhumation

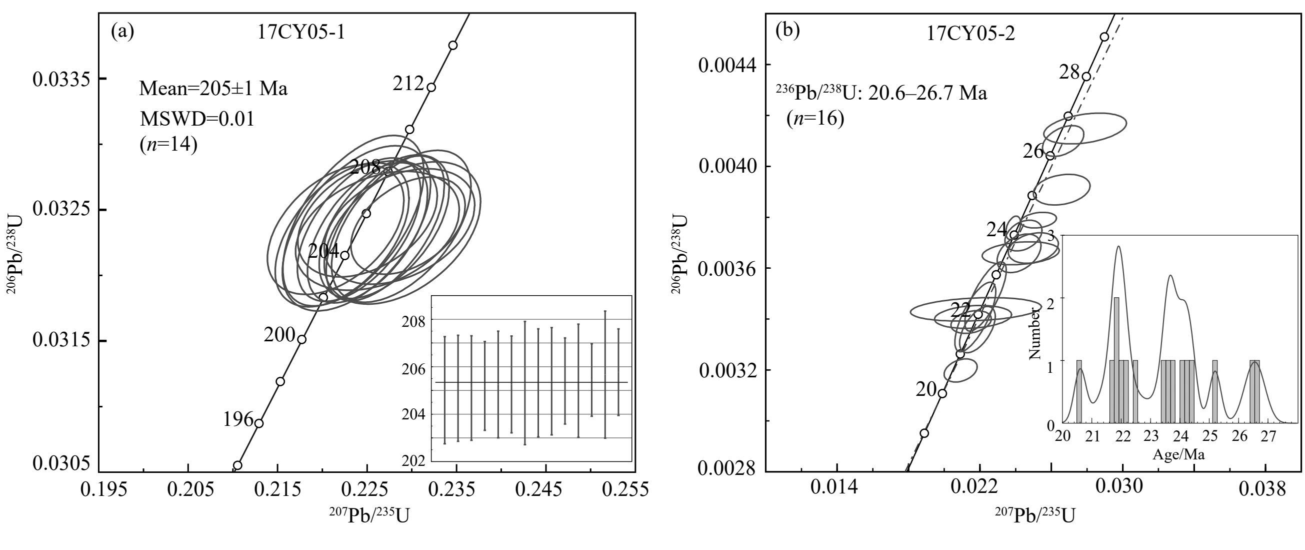

Fig. 9. a−Zircon U-Pb concordia diagrams and $^{206}Pb/^{238}U$ weighted mean age of Sample 17CY05-1; b−zircon U-Pb concordia diagrams and cumulative Gaussian plus histogram plots of Sample 17CY05-2.

and/or cooling event at temperature of 320±40°C after high temperature deformation of the rocks.

Both muscovites and biotites were separated from the sample 17CY05-1 for Ar-Ar dating. The total gas age of muscovites is 16.64 Ma, and 10 steps from 800°C to 1400°C comprise a well-defined age plateau (Fig. 10e). The plateau age is 16.56 ± 0.21 Ma, corresponding to 99.3% of ^{39}Ar release. The $^{36}Ar/^{40}Ar$-$^{39}Ar/^{40}Ar$ isochrone age is 16.47 ±

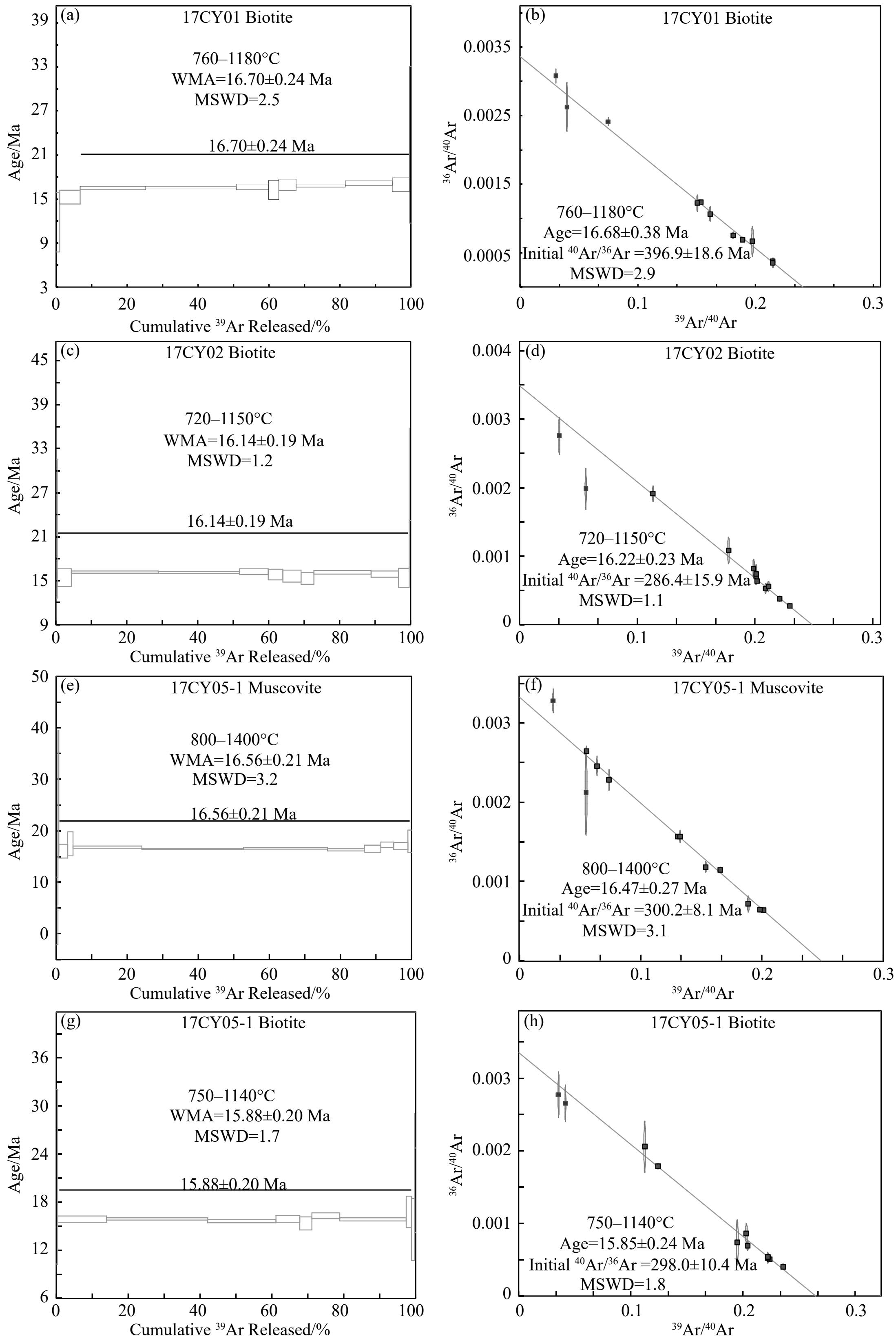

Fig. 10. $^{40}Ar/^{39}Ar$ plateau age and $^{36}Ar/^{40}Ar$-$^{39}Ar/^{40}Ar$ isochron age of biotite and muscovite from samples in the Demala Group complex. WMA–weighted mean age; MSWD–mean square of weighted deviates.

0.27 Ma (Fig. 10f). The initial $^{40}Ar/^{36}Ar$ is 300.2 ± 8.1 (MSWD=3.1), slightly higher than Nier value, indicating the presence of slightly excess argon. The total gas age of biotites is 15.92 Ma, and nine steps from 750°C to 1140°C comprise a well-defined age plateau (Fig. 10g). The plateau age is 15.88 ± 0.20 Ma, corresponding to 99.4% of ^{39}Ar release. The $^{36}Ar/^{40}Ar$-$^{39}Ar/^{40}Ar$ isochrone age is 15.85 ± 0.24 Ma (Fig. 10h). The initial $^{40}Ar/^{36}Ar$ is 298.0 ± 10.4 (MSWD=1.8), comparable to Nier value, indicating that there is no excess argon. According to microscopic observation, the muscovites and biotites in the sample are arranged in the direction consistent with the gneissic foliation and the stretching lineation of other minerals such as feldspar and quartz (Fig. 3d). This indicates that the muscovites and biotites were formed as a result of deformation and metamorphism at the temperature of 550−650°C. The closure temperatures for muscovite and biotite Ar-Ar isotopic systems are 450±50°C and 320±40°C, respectively (Harrison TM et al., 1985; Hames WE and Bowring SA, 1994), lower than deformation temperature of the sample. Therefore, the mica Ar-Ar ages of the sample 17CY05-1 can reveal the exhumation and/or cooling history of the rocks.

As for the sample 17CY05-2, the muscovites were selected for $^{40}Ar/^{39}Ar$ dating. The total gas age is 16.88 Ma, and 13 steps from 650°C to 1400°C comprise a well-defined age plateau (Fig. 11a). The plateau age is 16.90 ± 0.21 Ma, corresponding to 100% of ^{39}Ar. The $^{36}Ar/^{40}Ar$-$^{39}Ar/^{40}Ar$ isochrone age is 16.92 ± 0.25 Ma (Fig. 11b). The initial $^{40}Ar/^{36}Ar$ is 294.4 ± 6.3 (MSWD=2.4), comparable to Nier value, indicating that there is no excess argon. The sample 17CY05-2 was taken from the leucogranite vein cutting through the sample 17CY05-1 (Fig. 2f). The development of muscovites was related to anatexis at high temperature above 700°C. Hence, the Ar-Ar age results represent the time when the rocks were uplifted and cooled to a temperature of about 450±50°C after anatexis.

Biotites separated from the sample 17CY06-1 were chosen for $^{40}Ar/^{39}Ar$ dating. The total gas age is 14.42 Ma, and 11 steps from 650°C to 1160°C comprise a well-defined age plateau (Fig. 11c). The plateau age is 14.39 ± 0.20 Ma, corresponding to 99.7% of ^{39}Ar release. The $^{36}Ar/^{40}Ar$-$^{39}Ar/^{40}Ar$ isochrone age is 14.41 ± 0.23 Ma (Fig. 11d). The initial $^{40}Ar/^{36}Ar$ is 293.7 ± 8.0 (MSWD=2.7), comparable to Nier value, indicating that there is no excess argon. The sample consists of granitic gneiss. As indicated by field outcrops, the biotite aggregates are discontinuously arranged along the gneissic foliation (Figs. 2i,j), indicating that the development of biotites was related to metamorphism and deformation at high temperature about 550−650°C. The Ar-Ar age of biotites represents the time when the rocks cooled to 320 ± 40°C.

Muscovites were separated from the sample 17CY09-2 for Ar-Ar dating. The total gas age is 24.08 Ma, and six steps from 870°C to 1110°C comprise a well-defined age plateau (Fig. 11e). The plateau age is 23.40 ± 0.31 Ma, corresponding to 76.0% of ^{39}Ar release. The $^{36}Ar/^{40}Ar$-$^{39}Ar/^{40}Ar$ isochrone age is 23.13 ± 1.00 Ma (Fig. 11f). The initial 312.9 ± 63.3 (MSWD=2.9), higher than Nier value, indicating the presence of excess argon. According to microscopic observation, the muscovite aggregates are arranged parallel to the gneissic foliation and the stretching lineation of other minerals such as feldspar and quartz (Fig. 3f). This indicates that the formation of muscovites was the result of deformation and metamorphism on the condition of 550−650°C. Based on the closure temperatures for muscovite Ar-Ar isotopic systems, the Ar-Ar age indicates the time when the sample cooled to 450 ± 50°C.

5. Discussion

5.1. Composition and ages of protoliths of the Demala Group complex

The zircon U-Pb ages of the two granitic gneiss samples in this paper are 218 ± 1 Ma and 205 ± 1 Ma each. Although the samples have been modified by metamorphism and deformation, the CL images of the most zircons still show the characteristics of magmatic crystallization zoning. The zircon Th/U ratios are greater than 0.1, indicating the characteristics of magmatic zircons (Wu YB and Zheng YF, 2004). In terms of microscopic structural features of the granitic gneiss, the quartz in the granitic gneiss appears as polycrystalline ribbons, and feldspar in the granitic gneiss is porphyroclastic in shape and shows bulging and recrystallized new grains (Figs. 3d, f). All these jointly reveal that the rocks mainly deformed at medium temperatures (550−650°C, amphibolite facies), below the diffusion and closure temperatures of Pb in the zircons (ca. 900°C, Lee JK et al., 1997; Cherniak DJ and Watson EB, 2000). Therefore, the deformation did not destroy the U-Pb isotope system of the zircons, further indicating that the U-Pb ages 218 ± 1 Ma and 205 ± 1 Ma of the granitic gneiss samples can represent the magma crystallization age of their protoliths (granite). In terms of the studies on Mesozoic-Cenozoic granite ages in Chayu area, the ages previously reported are mostly Late Jurassic-Early Cretaceous (153−113 Ma) and the Paleocene (64−59 Ma) (Chiu HY et al., 2009; Zhu DC et al., 2009; Pan FB et al., 2012), with no reports on Early Mesozoic granite. Dong YS et al., (2011) obtained the protolith age of 217 Ma from the biotite-hornblende schist of the Demala Group complex and interpreted that this age may represent the age of intermediate-basic magmatism of Late Triassic in the area. In this study, the granite emplacement age of 218−205 Ma was obtained, indicating again that Indosinian or Early Mesozoic magmatic activities ever occurred in Chayu area. Previous researchers have successively reported the ages of Indosinian granodiorite or great numbers of Indosinian inherited zircons in Luozha (Li C et al., 2003), Menba (He ZH et al., 2006), Nanmulin (Chu MF et al., 2006) and Nyainqentanglha (Kapp JLD et al., 2005) areas in the middle part of Lhasa Block and taken them as the evidence of northward subduction of Neo-Tethys Ocean in the Late Triassic. In recent years, Paleo-Tethys high-pressure eclogites (Yang JS et al., 2007) and

Indosinian collisional orogenic events (Li HQ et al., 2008, 2012; Li GM et al., 2020) were discovered in Sumdo area in the middle part of Lhasa Block, revealing the presence of Paleo-Tethys basin in Lhasa Block and new information about collisional orogeny between southern and northern blocks. Was the Late Triassic magmatism in the Chayu area related to the northward subduction of the Neo-Tethys ocean plate or to the subduction-collision orogeny of the Paleo-Tethys ocean newly discovered in the Lhasa Block? Further study on petrogeochemistry is needed.

The zircons from two samples of the banded biotite quartzofeldspathic gneiss have core-rim structure. The cores of zircon are not affected by metamorphism, which preserve the characteristics of zircons in protolith. The rims were formed owing to later metamorphism. This is also revealed by the Th and U content and Th/U ratios of the zircons. The rims of zircon have relatively high U content, relatively low Th content and low Th/U ratios (< 0.1) (Figs. 6b, f), showing the characteristiccs of metamorphic zircons (Wu YB and Zheng YF, 2004). Therefore, the U-Pb ages of zircon rims of the two samples, i.e., 203 ± 2 Ma (17CY01) and 190 ± 1 Ma (17CY09-1), represent the metamorphism ages of the quartzofeldspathic gneiss. The Chayu area underwent Late Triassic magmatic activities as mentioned above; therefore the metamorphism during 203−190 Ma may be related to the tectonic-magmatic activities in the same period. Since the

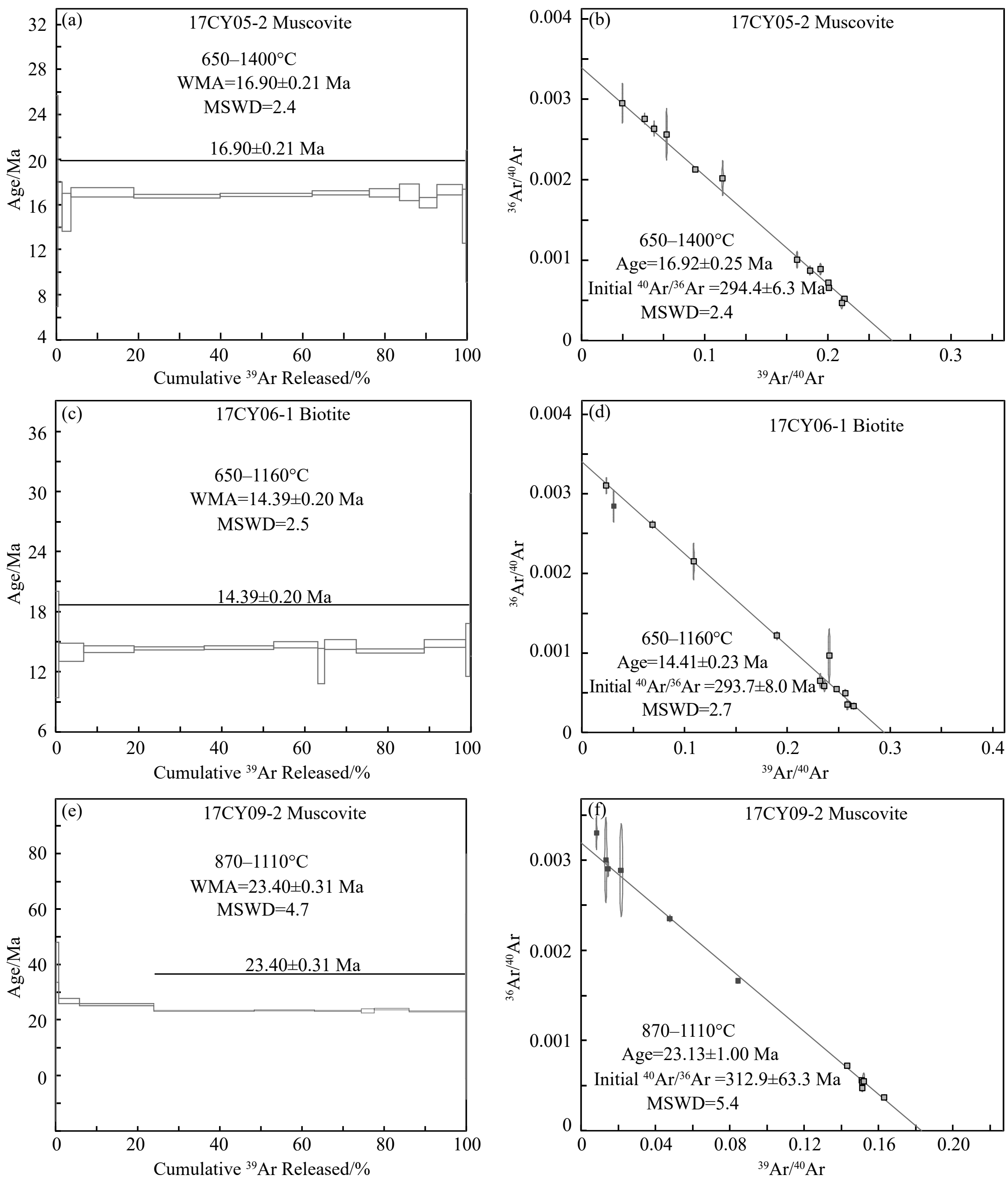

Fig. 11. $^{40}Ar/^{39}Ar$ plateau age and $^{36}Ar/^{40}Ar$-$^{39}Ar/^{40}Ar$ isochron age of biotite and muscovite from samples in the Demala Group complex. WMA–weightedmean age; MSWD–mean square of weighted deviates.

protoliths of the banded biotite quartzofeldspathic gneiss are clastic sedimentary rocks, the U-Pb age data of their zircon cores can reflect the sedimentary time and provenance information of the protoliths. In this paper, statistical analysis was made for the detrital zircon ages of these two samples and the U-Pb age data of detrital zircons from the biotite-quartz gneiss of the Demala Group complex obtained by Dong YS et al. (2011). As shown in the statistic histogram (Fig. 12), the detrital zircon ages are distributed in the range of 3284−314 Ma (n=94) and the ages of several youngest zircons are mainly 391−314 Ma, indicating that the protoliths of this set of paragneiss were deposited in the Early Carboniferous or later. Meanwhile, the age distribution characteristics of the detrital zircons can provide important constraints on provenance areas. The detrital zircon ages of the Demala Group complex mainly fall in a few age groups, namely 644−446 Ma (n=32), 1213−865 Ma (n=29), and 1780−1400 Ma (n=10), which are common in the detrital zircons of the Tethys-Himalayan sedimentary rock series (DeCelles PG et al., 2000; Gehrels GE et al., 2003; Myrow PM et al., 2003). According to the dating of detrital zircons in the Nyingchi Group that lies to the west of the Nameche Barwa Syntaxis (Dong X et al., 2009), the ages obtained are also distributed in 500−600 Ma and 900−1200 Ma. The 644−446 Ma age of detrital zircons from the Demala Group complex is comparable to the timing of the Pan-African orogeny in the Gondwanaland (ca. 550 Ma), indicating that the Early Paleozoic granites widely developed in the north margin of the East Gondwanaland (520−490 Ma) may have provided a large amount of detrital zircons as provenance (Xu ZQ et al., 2005; Zhang ZM et al., 2008, 2012b; Dong X et al., 2010; Wang XX et al., 2012; Zhu DC et al., 2012). In contrast, the ages 1213−865 Ma records the Greenville movement of the East Gondwanaland (ca. 1100 Ma). In addition, the zircons from the sample 17CY09-1 yield a set of ages of around 205 Ma. Meanwhile, these zircons are mostly magmatic zircons with a high euhedral degree. Given the presence of magmatic intrusion of around 205 Ma in the area, the ages (ca. 205 Ma) may be unrelated to the rocks in the provenance but are probably related to magmatic activities in the same period.

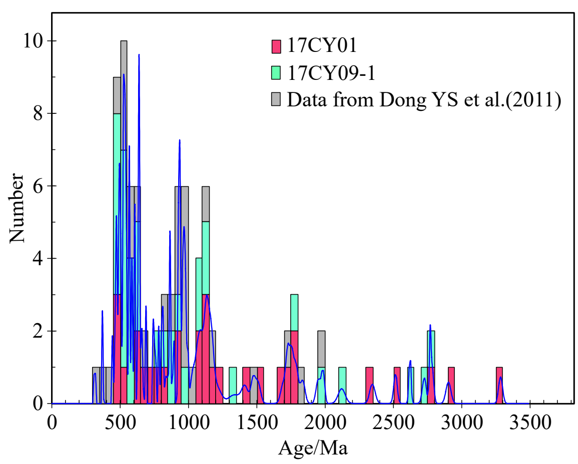

Fig. 12. Frequency plot diagram of the detrital zircon U-Pb ages of the Demala Group complex.

5.2. Deformation age of the Demala Group complex and its implications for regional geology

A series of leucogranite veins (Figs. 2e−h) have developed in the gneiss of the Demala Group complex. Some of them are parallel to the foliation of gneiss (Fig. e), and some of them cut through the foliation (Figs. 2f, h). The veins vary in width, from ca. 10 cm to up to ca. 2 m. Some of the veins extend regularly along with the gneissic foliation, while others extend shortly and wedge out. They show no intrusive relation with host rocks, without baked or chilled edge. It can be observed that they encapsulate host rocks locally. In terms of mineral composition, they mainly consist of feldspar and quartz, as well as a small quantity of muscovite. As shown from the zircon CL image of the leucogranite vein sample (17CY05-2), their zircons are weakly luminous in general (Fig. 8c), which is probably because of the low Th content and high U content (Keay S et al., 2001; Rubatto D, 2002; Wu YB and Zheng YF, 2004). In terms of the inner structural characteristics of the zircons, most zircon crystals show fog-like or spongy inside, with the oscillatory zoning texture still visible on zircon rims. In terms of trace elements, the zircons of the leucogranite veins generally show low Th/U ratios (< 0.05; Table S2), while the zircons of the host rocks (orthogneiss) have relatively high Th/U ratios. All these indicate that the zircons in the leucogranite vein sample 17CY05-2 were formed owing to anatexis, further proving that the anatexis in the Demala Group complex mainly occurred in 22−24 Ma.

The plateau ages of three muscovite samples in this paper are 16.56 ± 0.21 Ma, 16.90 ± 0.21 Ma, and 23.40 ± 0.31 Ma, and the plateau ages of four biotite samples are 16.70 ± 0.24 Ma, 16.14 ± 0.19 Ma, 15.88 ± 0.20 Ma, and 14.39 ± 0.20 Ma. According to microscopic observation, these mica minerals either develop around feldspar porphyroclasts (Figs. 3b, c, f) or are arranged parallel to quartz ribbons (Figs. 3d, e). Besides, some mica minerals develop in the shape of mica fish (Fig. 3b), serving as an indicator of dextral shear. therefore, the development of mica minerals were due to the deformation at medium to high temperature (550−650°C, amphibolite facies), which is higher than the closure temperatures for muscovite and biotite Ar-Ar isotopic systems (450 ± 50°C and 320 ± 40°C respectively; Harrison TM et al., 1985; Hames WE and Bowring SA, 1994). The Ar-Ar age results reveal that the time when the Demala Group complex was exhumated from the deep crust and cooled to the temperature of 320±40°C, is about 16−14 Ma.

As indicated by previous research data, the Cenozoic intracontinental deformation in Chayu area is mainly characterized by the development of a series of strike-slip shear faults in NW-SE strike. Among them, the Parlung and Puqu strike-slip faults are considered to be branches of Jiali fault zone (Lee HY et al., 2003), which is one of the most important strike-slip faults in the southern part of Qinghai-Tibet Plateau. The development of the Jiali fault zone was directly affected by the large-scale southeastward escape of crustal materials and block rotation in the area from the Jinsha, Lancang, and Nujiang rivers in eastern Tibet to Indochina region after the India-Eurasia collision (Tapponnier P et al., 1986, 1990; Lee TY et al., 1994; Chen HH et al., 1995; Sato K et al., 1999, 2001; Qiu RZ et al., 2018). As shown by previous tectono-thermochronology data, the dextral ductile-brittle shear in the Jiali fault zone started at ca. 24 Ma and lasted to ca. 12 Ma (Lee HY et al., 2003; Lin TH et al., 2009; Zhang B et al., 2020), coinciding with the ages of anatexis and subsequent uplifting-exhumation in the Demala Group complex. In summary, the anatexis and uplifting-exhumation of the Demala Group complex in Chayu area since the Cenozoic (24−14 Ma) are related to the shearing in Jiali strike-slip fault zone, and serve as tectonic response to the large-scale southeastward escape of crustal materials and block rotation in southeastern Tibet after the India-Eurasia collision.

6. Conclusions

(i) The Demala Group complex should be a set of metamorphic complexes. Besides Precambrian basement metamorphic rock series, the protoliths of the Demala Group complex also include Paleozoic sedimentary rocks and Mesozoic granitic rocks. Meanwhile, owing to the deformation and metamorphism during the Late Mesozoic-Cenozoic, the protoliths were modified and appear as present gneiss-schist.

(ii) According to zircon U-Pb dating in this paper, the zircon U-Pb ages of two granitic gneiss samples are 218±1 Ma and 205±1 Ma, representing the magmatic crystallization ages of granite and indicating that the Late Triassic magmatic activities occurred in Chayu area.

(iii) Considering the data of two samples taken from the banded biotite quartzofeldspathic gneiss as well as previous data, the detrital zircon ages of the protoliths of the paragneiss in the Demala Group complex indicate that this set of paragneisses were deposited in the Early Carboniferous or later. Furthermore, the detrital zircon ages of 644–446 Ma and 1213–865 Ma can be the records of the Pan-African orogeny in the Gondwanaland (ca. 550 Ma) and the Greenville movement of the East Gondwanaland (ca. 1100 Ma), respectively.

(iv) As indicated by the U-Pb ages of the zircons of metamorphism genesis and the $^{40}Ar/^{39}Ar$ chronological data of mica minerals, two stages of the metamorphism and deformation can be revealed in the Demala Group complex since the Mesozoic, namely Late Triassic-Early Jurassic (203–190 Ma) and Oligocene-Miocene (24–14 Ma). The early stage of metamorphism was related to the Late Triassic tectono-magmatism in the area. In contrast, the anatexis and uplifting-exhumation of the late stage (24–14 Ma) were related to the shearing of the Jiali strike-slip fault zone.

CRediT authorship contribution statement

Yuan Tang and Yu-ping Liu conceived of the presented idea. Yuan Tang and Peng Wang carried out the experiments. Wen-qing Tang and Ya-dong Qin contributed to sample collection. Yuan Tang and Xiao-dong Gong contributed to the figures. Yuan Tang, Dong-bing Wang and Bao-di Wang contributed to the interpretation of the results. Yuan Tang took the lead in writing the manuscript. All authors provided critical feedback and helped shape the research, analysis and manuscript.

Declaration of competing interest

The authors declare no conflicts of interest.

Acknowledgment

This study was jointly funded by a project of National Natural Science Foundation of China (41773026) and two geological survey projects initiated by the China Geological Survey (DD20190053, DD20160021).

Supplementary dataset

Supplementary dataset (Table S1, Table S2, Table S3) to this article can be found online at doi: 10.31035/cg2021021.

References

BGMRXR [Bureau of Geology and Mineral Resources of Xizang Autonomous Region. Regional Geology of Xizang (Tibet) Autonomous Region]. 1993. Beijing, Geological Publishing House (in Chinese with English abstract).

Chen HH, Dobson J, Heller F, Hao J. 1995. Paleomagnetic evidence for clockwise rotation of the Simao region since the Cretaceous: A consequence of India-Asia collision. Earth and Planetary Science Letters, 134(l−2), 203–217. doi: 10.1016/0012-821X(95)00118-V.

Chen W, Zhang Y, Zhang YQ, Jin GS, Wang QL. 2006. Late Cenozoic episodic uplifting in southeastern part of the Tibetan plateau-evidence from Ar-Ar thermochronology. Acta Petrologica Sinica, 22(4), 867–872 (in Chinese with English abstract). doi: 10.1016/j.sedgeo.2005.11.021.

Cherniak DJ, Watson EB. 2000. Pb diffusion in zircon. Chemical Geology, 172(1−2), 5–24. doi: 10.1016/S0009-2541(00)00233-3.

Chiu HY, Chung SL, Wu FY, Liu DY, Liang YH, Lin IJ, Iizuka Y, Xie LW, Wang YB, Chu MF. 2009. Zircon U-Pb and Hf isotopic constraints from eastern Transhimalayan batholiths on the recollisional magmatic and tectonic evolution in southern Tibet. Tectonophysics, 477(1−2), 3–19. doi: 10.1016/j.tecto.2009.02.034.

Chu MF, Chung SL, Song B, Liu DY, O’Reilly SY, Pearson NJ, Ji JQ, Wen DJ. 2006. Zircon U-Pb and Hf isotope constraints on the Mesozoic tectonics and crustal evolution of southern Tibet. Geology, 34(9), 745–748. doi: 10.1130/G22725.1.

DeCelles PG, Gehrels GE, Quade J, LaReau B, Spurlin M. 2000. Tectonic implications of U-Pb zircon ages of the Himalayan Orogenic Belt in Nepal. Science, 288, 497–499. doi: 10.1126/science.288.5465.497.

Ding HX, Zhang ZM, Dong X, Yan R, Lin YH, Jiang HY. 2015. Cambrian ultrapotassic rhyolites from the Lhasa terrane, south Tibet: Evidence for Andean-type magmatism along the northern active margin of Gondwana. Gondwana Research, 27, 1616–1629. doi: 10.1016/j.gr.2014.02.003.

Dong HW, Xu ZQ, Li Y, Liu Z. 2014. Zircon LA-ICP-MS U-Pb dating of the triassic anatexis at Mutuo, the Eastern Himalayan Syntaxis. Geotectonica et Metallogenia, 38(2), 398–407. doi: 10.1007/s00531-014-1057-y.

Dong X, Zhang ZM, Santosh M. 2010. Zircon U-Pb chronology of the Nyingchi group, southern Lhasa terrane, Tibetan plateau:

Implications for Grenvillian and Pan-African provenance and Mesozoic-Cenozoic metamorphism. The Journal of Geology, 118, 677–690. doi: 10.1086/656355.

Dong X, Zhang ZM, Wang JL, Zhao GC, Liu F, Wang W, Yu F. 2009. Provenance and formation age of the Nyingchi Group in the southern Lhasa terrane, Tibetan Plateau: Petrology and zircon U-Pb geochronology. Acta Petrologica Sinica, 25(7), 1678–1694 (in Chinese with English abstract). doi: 10.1016/S1874-8651(10)60080-4.

Dong YS, Li C, Chen H, Chen W, Zhang Y. 2011. Study on geochronology and its geological significance of the Demala Group complex in Chayu area, Southeast Tibetan Plateau. Acta Petrologica Sinica, 27(4), 1198–1208 (in Chinese with English abstract). doi: 10.1007/s11589-011-0776-4.

Gehrels GE, DeCelles PG, Martin A, Ojha TP, Pinhassi G. 2003. Initiation of the Himalayan Orogen as an Early Paleozoic thin-skinned thrust belt. GSA Taday, 13, 4–9.

Hames WE, Bowring SA. 1994. An empirical evaluation of the argon diffusion geometry in muscovite. Earth and Planetary Science Letters, 124, 161–167. doi: 10.1016/0012–821X(94)00079–4.

Hames WE, Bowring SA. 1994. An empirical evaluation of the argon diffusion geometry in muscovite. Earth and Planetary Science Letters, 124, 161–167. doi: 10.1016/0012-821X(94)00079-4.

Harrison TM, Duncan I, Mcdougall I. 1985. Diffusion of ^{40}Ar in biotite: Temperature, pressure and compositional effects. Geochimica et Cosmochimica Acta, 49, 2461–2468. doi: 10.1016/0016-7037(85)90246-7.

He SP, Li RS, Wang C, Gu PY, Yu PS, Shi C, Zha XF. 2012. The determination of the age of Jiayuqiao Group in northern Gangdise of Tibetan Plateau. Geology in China, 39, 21–28 (in Chinese with English abstract).

He ZH, Yang DM, Zheng CQ, Wang TW. 2006. Isotopic dating of the Mamba granitoid in the Gangdise tectonic belt and its constraint on the subduction time of the Neotethys. Geological Review, 52(1), 100–106 (in Chinese with English abstract). doi: 10.1007/s11442-006-0415-5.

Hu DG, Wu ZH, Ye PS, Jiang W. 2003. SHRIMP U-Pb ages of zircons from dioritic gneiss in the Nyainqentanglha Mountains, Tibet. Geological Bulletin of China, 22, 936–940.

Hu DG, Wu ZH, Jiang W, Shi YR, Ye P. 2005. SHRIMP zircon U-Pb age and Nd isotopic study on the Nyainqentanglha Group in Tibet. Science in China Series D-Earth Sciences, 48, 1377–1386. doi: 10.1360/04yd0183.

Hu PY, Li C, Wang M, Xie CM, Wu YW. 2013. Cambrian volcanism in the Lhasa terrane, southern Tibet: Record of an early Paleozoic Andean-type magmatic arc along the Gondwana proto-Tethyan margin. Journal of Asian Earth Sciences, 77, 91–107. doi: 10.1016/j.jseaes.2013.08.015.

Hu PY, Zhai QG, Tang Y, Wang J, Wang HT. 2016. Early Neoproterozoic meta-gabbro (~925 Ma) from the Lhasa terrane, Tibetan Plateau and its geological significance. Chinese Science Bulletin, 61(19), 2176–2186 (in Chinese with English abstract). doi: 10.1360/N972016-00143.

Hu ZC, Zhang W, Liu YS, Gao S, Li M, Zong KQ, Chen HH, Hu SH. 2015. “Wave” signal smoothing and mercury removing device for laser ablation quadrupole and multiple collector ICP-MS analysis: Application to lead isotope analysis. Analytical Chemistry, 87, 1152–1157. doi: 10.1021/ac503749k.

Kapp JLD, Harrison TM, Kapp P, Grove M, Lovera OM, Lin D. 2005. Nyainqentanglha Shan: A window into the tectonic, thermal, and geochemical evolution of the Lhasa block, southern Tibet. Journal of Geophysical Research, 110(B08043), 1–23. doi: 10.1029/2004JB003330.

Keay S, Lister G, Buick I. 2001. The timing of partial melting, Barrovian metamorphism and granite intrusion in the Naxos metamorphism core complex, Cyclades, Aegean Sea, Greece. Tectonophysics, 342(3−4), 275–312. doi: 10.1016/S0040-1951(01)00168-8.

Lee HY, Chung SL, Wang JR, Wen AJ, Lo CH, Yang TF, Zhang YQ, Xie YW, Lee TY, Wu GY, Ji JQ. 2003. Miocene Jiali faulting and its implications for Tibetan tectonic evolution. Earth and Planetary Science Letters, 205(3−4), 185–194. doi: 10.1016/S0012-821X(02)01040-3.

Lee JK, Williams IS, Ellis DJ. 1997. Pb, U and Th diffusion in natural zircon. Nature, 390(6656), 159–162. doi: 10.1038/36554.

Lee TY, Lawver LA. 1994. Cenozoic plate reconstruction of the South China Sea region. Tectonophysics, 235(1−2), 149–180. doi: 10.1016/0040-1951(94)90022-1.

Li C, Wang TW, Li HM, Zeng QG. 2003. Discovery of Indosinian megaporphyritic granodiorite in the Gangdise area: Evidence for the existence of Paleo Gangdise. Geological Bulletin of China, 22(5), 364–366 (in Chinese with English abstract). doi: 10.1016/S0955-2219(02)00073-0.

Li GM, Zhang LK, Wu JY, Xie CM, Zhu LD, Han FL. 2020. Reestablishment and scientific significance of the Ocean plate geology in the Southern Tibet Plateau, China. Sedimentary Geology and Tethyan Geology, 40(1), 1–14 (in Chinese with English abstract).

Li HQ, Cai ZH, Chen SY, Tang ZM, Yang M. 2008. The Indosinian orogenesis occurred in Lhasa terrain and the evidence from muscovite ^{40}Ar-^{39}Ar geochronology. Acta Petrologica Sinica, 24(7), 1595–1604 (in Chinese with English abstract). doi: 10.2113/gssajg.116.1.169.

Li HQ, Xu ZQ, Yang JS, Tang ZM. 2012. Indosinian orogenesis in the Lhasa Terrane, Tibet: New muscovite ^{40}Ar-^{39}Ar geochronology and evolutionary process. Acta Geologica Sinica, 86(5), 1116–1127. doi: 10.1111/j.1755-6724.2012.00735.x.

Li P. 1955. Novice understanding of the geology of eastern Tibet. Chinese Science Bulletin, 7, 62–71 (in Chinese with English abstract).

Li YC, Zhang KX, He WH, Xu YD, Song BW, Yu Y, Ke X, Kou XH, Luo MS, Xin HT, Fu JY, Yang ZL, Zhao XM, Yin FG, Li ZP. 2018. Division of tectonic-strata superregions in China. China Geology, 2, 236–256. doi: 10.31035/cg2018028.

Lin TH, Lo CH, Chung SL, Hsu FJ, Yeh MW, Lee TY, Ji JQ, Wang YZ, Liu DY. 2009. ^{40}Ar/^{39}Ar dating of the Jiali and Gaoligong shear zones: Implications for crustal deformation around the Eastern Himalayan Syntaxis. Journal of Asian Earth Sciences, 34(5), 674–685. doi: 10.1016/j.jseaes.2008.10.009.

Lin YH, Zhang ZM, Dong X, Shen K, Lu X. 2013. Precambrian evolution of the Lhasa terrane, Tibet: Constraint from the zircon U-Pb geochronology of the gneisses. Precambrian Research, 237, 64–77. doi: 10.1016/j.precamres.2013.09.006.

Liu YS, Gao S, Hu ZC, Gao CG, Zong KQ, Wang DB. 2010. Continental and oceanic crust recycling-induced melt-peridotite interactions in the Trans-North China Orogen: U-Pb dating, Hf isotopes and trace elements in zircons of mantle xenoliths. Journal of Petrology, 51, 537–571. doi: 10.1093/petrology/egp082.

Liu YS, Hu ZC, Gao S, Günther D, Xu J, Gao CG, Chen HH. 2008. In situ analysis of major and trace elements of anhydrous minerals by LA-ICP-MS without applying an internal standard. Chemical Geology, 257, 34–43. doi: 10.1016/j.chemgeo.2008.08.004.

Ludwig KR. 2003. ISOPLOT 3.00: A Geochronological Toolkit for Microsoft Excel. Berkeley Geochronology Center, California, Berkeley, 39.

Luo JN, Zhang ZG, Chen M, Li GM, Tong ZX. 1992. Sedimentary Geology and Minelalization in the Tethys of the Nujiang-Lancanganjiang-Jinshajiang area. Beijing, Geological Publishing House (in Chinese).

Myrow PM, Hughes NC, Paulsen TS, Williams IS, Parcha SD, Thompson KR, Bowering SA, Peng SC, Ahluwalia AD. 2003. Integrated tectonostratigraphic analysis of the Himalaya and implications for its tectonic reconstruction. Earth and Planetary Science Letters, 212, 433–443. doi: 10.1016/S0012-821X(03)00280-2.

Pan FB, Zhang HF, Harris N, Xu WC, Guo L. 2012. Oligocene magmatism in the eastern margin of the East Himalayan Syntaxis and its implication for the India-Asia post-collisional process. Lithos, 154, 181–192. doi: 10.1016/j.lithos.2012.07.004.

Pan XP, Li RS, Wang C, Yu PS, Gu PY, Zha XF. 2012. Geochemical characteristics of the Cambrian volcanic rocks in Banglecun area on the northern margin of Gangdise, Nyima County, Tibet. Geological Bulletin of China, 31(1), 63–74 (in Chinese with English abstract).

Peng XJ, Chen YM, Zhang SQ. 1999. Paleoproterozoic Demala Group-complex in the Chayu area, Tibet. Regional Geology of China, 18(2), 148–154 (in Chinese with English abstract).

Qiu RZ, Ludington SD, Zhou S, Tan YJ, Yan GS, Liu ZG, Chen XF, Zhu QL, Qiu L, Ren XD, Zhao LK. 2018. Discussion on the dextral movement and its effect in continental China and adjacent areas since Cenozoic. China Geology, 4, 522–539. doi: 10.31035/cg2018056.

Rubatto D. 2002. Zircon trace element geochemistry: Partitioning with garnet and the link between U-Pb ages and metamorphism. Chemical Geology, 184(1−2), 123–138. doi: 10.1016/S0009-2541(01)00355-2.

Sato K, Liu YY, Zhu ZC, Yang ZY, Otofuji Y. 1999. Paleomagnetic study of Middle Cretaceous rocks from Yunlong, western Yunnan, China: Evidence of southward displacement of Indochina. Earth and Planetary Science Letters, 165(1), 1–15. doi: 10.1016/S0012-821X(98)00257-X.

Sato K, Liu YY, Zhu ZC, Yang ZY, Otofuji Y. 2001. Tertiary paleomagnetic data from northwestern Yunnan, China: Further evidence for large clockwise rotation of the Indochina block and its tectonic implications. Earth and Planetary Science Letters, 185(1−2), 185–198. doi: 10.1016/S0012-821X(00)00377-0.

Steiger RH, Jager E. 1977. Subcommission on geochronology: Convention on the use of decay constants in geo-and cosmochronology. Earth and Planetary Science Letters, 36, 359–362. doi: 10.1016/0012-821X(77)90060-7.

Tang Y, Wang DB, Liao SY, Wang BD, Yin FG, Wang LQ. 2016. Geochronological characterization and regional tectonic implication of the leucogranites in the southern segment of Gaoligong metamorphic zone, Western Yunnan. Acta Petrologica Sinica, 32(8), 2347–2366 (in Chinese with English abstract).

Tang Y, Wang DB, Liao SY, Wang BD, Yin FG. 2020. Fabrics and $^{40}Ar/^{39}Ar$ ages of metamorphic rocks in the Gaoligong tectonic belt: Implications for Cenozoic metamorphism and deformation in the SE Tibetan Plateau. Journal of Asian Earth Sciences, 192. doi: 10.1016/j.jseaes.2020.104270.

Tapponnier P, Lacassin R, Leloup PH, Schärer U, Zhong DL, Liu XH, Ji SC, Zhang LS, Zhong JY. 1990. The Ailao Shan/Red River metamorphic belt: Tertiary left-lateral shear between lndochina and South China. Nature, 343, 431–437. doi: 10.1038/343431a0.

Tapponnier P, Peltzer G, Armijo R. 1986. On the mechanics of the collision between India and Asia. In: Coward MP, Ries AC (eds.), Collision Tectonics. Geological Society of London Special Publication, 19, 115−157.

Wang XX, Zhang JJ, Santosh M, Liu J, Yan SY, Guo L. 2012. Andean-type orogeny in the Himalayas of south Tibet: Implication for early Paleozoic tectonics along the Indian margin of Gondwana. Lithos, 154, 248–262. doi: 10.1016/j.lithos.2012.07.011.

Wu YB, Zheng YF. 2004. Genesis of zircon and its constranints on interpretation of U-Pb age. Chinese Science Bulletin, 49(15), 1554–1569. doi: 10.1007/BF03184122.

Xie YW, Peng XJ, Qiangbazhaxi, Xiluolangjie, Cirenyangjin. 2007. Recent progress in the study of the Neoproterozoic-Cambrian Bomi Group in the Bomi-Zayu area, eastern Tibet, China. Geological Bulletin of China, 26(1), 81–87 (in Chinese with English abstract).

Xu WC, Zhang HF, Harris N, Gu oL, Pan FB, Wang S. 2013. Geochronology and geochemistry of Mesoproterozoic granitoids in the Lhasa terrane, south Tibet: Implications for the early evolution of Lhasa terrane. Precambrian Research, 236, 46–58. doi: 10.1016/j.precamres.2013.07.016.

Xu ZQ, Yang JS, Liang FH, Qi XX, Liu FL, Zeng LS, Liu DY, Li HB, Wu CL, Shi RD, Chen SY. 2005. Pan-African and Early Paleozoic orogenic events in the Himalayan terrane: Inference from SHRIMP U-Pb zircon ages. Acta Petrologica Sinica, 21(1), 1–12 (in Chinese with English abstract). doi: 10.3321/j.issn:1000-0569.2005.01.001.

Yang JS, Xu ZQ, Li TF, Li HQ, Li ZL, Ren YF, Xu XZ, Chen SY. 2007. Oceanic subduction-type eclogite in the Lhasa block, Tibet, China: Remains of the Paleo-Tethys ocean basin? Geological Bulletin of China, 26(10), 1277–1287 (in Chinese with English abstract). doi: 10.1016/S1872-5791(07)60044-X.

Yin GH, Bao G, Yang SS, Hu QH. 2006. The granulites and ages of the Nyingchi Group Complex in the Nyingchi region, Xizang. Sedimentary Geology and Tethyan Geology, 26(3), 8–15 (in Chinese with English abstract).

Zhang B, Cai FL, Chen SY, Li XR, Zhang L. 2020. Sinistral strike-slip shearing along the Jiali shear zone around the Eastern Himalaya syntaxis region: Evidences for oligocene eastward limited translation of Tibet. Journal of Structural Geology, 139. doi: 10.1016/j.jsg.2020.104136.

Zhang XZ, Dong YS, Li C, Xie CM, Yang HT, Wang M. 2013. Delineation of Middle Neoproterozoic ophiolite mélange in the northern Lhasa terrane, South Tibet and its significance. Acta Petrologica Sinica, 29(2), 698–722 (in Chinese with English abstract).

Zhang Y, Chen W, Chen KL, Liu XY. 2006. Study on the Ar-Ar age spectrum of diagenetic I/S and the mechanism of ^{39}Ar recoil loss-Examples from the clay minerals of P-T boundary in Changxing, Zhejiang Province. Geological Review, 52(4), 556–561 (in Chinese with English abstract).

Zhang ZM, Dong X, Geng GS, Wang W, Yu F, Liu F. 2010. Precambrian metamorphism of the Northern Lhasa Terrane, South Tibet and its tectonic implications. Acta Geologica Sinica, 84(4), 449–456 (in Chinese with English abstract). doi: 10.1017/S0004972710001772.

Zhang ZM, Dong X, Liu F, Lin YH, Yan R, He ZY, Santosh M. 2012a. The making of Gondwana: Discovery of 650 Ma HP granulites from the North Lhasa, Tibet. Precambrian Research, 212−213, 107–116. doi: 10.1016/j.precamres.2012.04.018.

Zhang ZM, Dong X, Santosh M, Liu F, Wang W, Yiu F, He ZY, Shen K. 2012b. Petrology and geochronology of the NamcheBarwa Complex in the eastern Himalayan syntaxis, Tibet: Constraints on the origin and evolution of the north-eastern margin of the India Craton. Gondwana Research, 21, 123–137. doi: 10.1016/j.gr.2011.02.002.

Zhang ZM, Wang JL, Shen K, Shi C. 2008. Paleozoic circus-Gondwana orogens: Petrology and geochronology of the Namche Barwa Complex in the eastern Himalayan syntaxis, Tibet. Acta Petrologica Sinica, 24(7), 1627–1637 (in Chinese with English abstract). doi: 10.1016/j.sedgeo.2008.04.004.

Zhu DC, Mo XX, Wang LQ, Zhao ZD, Niu YL, Zhou CY, Yang YH. 2009. Petrogenesis of highly fractionated I-type granites in the Zayu area of eastern Gangdese, Tibet: Constraints from zircon U-Pb geochronology, geochemistry and Sr-Nd-Hf isotopes. Science in China (Series D), 52(9), 1223–1239. doi: 10.1007/s11430-009-0132-x.

Zhu DC, Zhao ZD, Niu YL, Dilek Y, Wang Q, Ji WH, Dong GC, Sui QL, Liu YS, Yuan HL, Mo XX. 2012. Cambrian bimodal volcanism in the Lhasa Terrane, southern Tibet: Record of an early Paleozoic Andean-type magmatic arc in the Australian proto-Tethyan margin. Chemical Geology, 328, 290–308. doi: 10.1016/j.chemgeo.2011.12.024.

Zong KQ, Klemd R, Yuan Y, He ZY, Guo JL, Shi XL, Liu YS, Hu ZC, Zhang ZM. 2017. The assembly of Rodinia: The correlation of early Neoproterozoic (ca. 900 Ma) high-grade metamorphism and continental arc formation in the southern Beishan Orogen, southern Central Asian Orogenic Belt (CAOB). Precambrian Research, 290, 32–48. doi: 10.1016/j.precamres.2016.12.010.